

DLR-IB-FA-BS-2018-92

**Fertigung, Untersuchung und
Bewertung von mehrteiligen
Preformen**

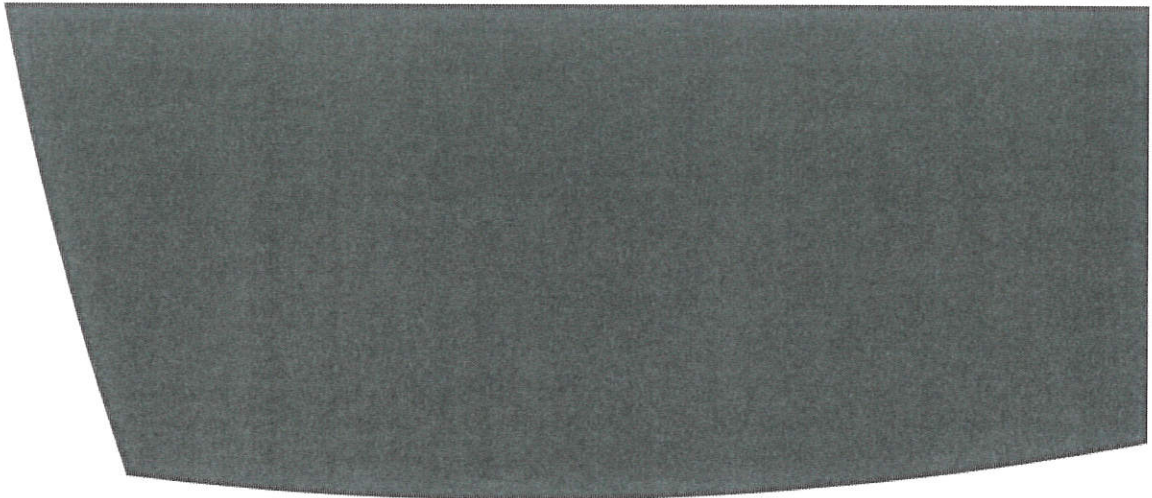
Studienarbeit

Aitor Ochotorena



DLR

**Deutsches Zentrum
für Luft- und Raumfahrt**



Institut für Faserverbundleichtbau und Adaptronik

DLR-IB-FA-BS-2018-92

**Fertigung, Untersuchung und Bewertung von
mehnteiligen Preformen**

Zugänglichkeit:

Stufe 1

Braunschweig, Mai 2018

Der Bericht umfasst: 84 Seiten

Institutsleiter:
Prof. Dr.-Ing. M. Wiedemann


Autor:
Aitor Ochotorena

Abteilungsleiter: 
Prof. Dr.-Ing. C. Hühne


Betreuer:
Alfred Tempel



Deutsches Zentrum
für Luft- und Raumfahrt



Technische
Universität
Braunschweig



Deutsches Zentrum
DLR für Luft- und Raumfahrt e.V.
Institut für Faserverbundleichtbau
und Adaptronik



Technische
Universität
Braunschweig

IAF

Fertigung, Untersuchung und Bewertung von mehrteiligen Preformen

Studienarbeit

an der Technischen Universität Braunschweig

Verfasser: Aitor Alejandro Ochotorena Esparcia
im Studiengang: Luft-und Raumfahrttechnik (M.Sc.)
Matr.-Nr.: 4859280

Erstprüfer:

Prof. Dr.-Ing. Christian Hühne (TU Braunschweig - IAF)

Betreuer:

Patrick Scholle M.Sc. (TU Braunschweig - IAF)

Betreuer:

Alfred Tempel M.Sc. (DLR)

Bearbeitungszeitraum: 15 Wochen

Abgabedatum 15.05.2018



Studienarbeit
für
Herrn Aitor Ochotorena
Matr. Nr. 4859280

Thema:

***Fertigung, Untersuchung und Bewertung von mehrteiligen
Preformen***

Zielsetzung:

Aktuelle Arbeiten am Deutschen Zentrum für Luft- und Raumfahrt haben zum Ziel, durch die Entwicklung eines automatisierten Preform-Konzeptes, Fertigungs- und Fügeprozesse in der Endlinienmontage zu beschleunigen und somit zu einer Reduzierung der gesamtheitlichen Kosten und Durchlaufzeiten beizutragen. Teilziel eines Projektes in enger Kooperation mit einem Flugzeughersteller ist ein seriennahes Industrialisierungskonzept, das die kontinuierliche Fertigung von Holmpreformen mit integrierter Lasteinleitungsfinne ermöglicht. Gegenstand dieser Studienarbeit ist die manuelle Fertigung von Subpreformen mit bereits fest definierter Geometrie zur späteren Zuführung in einen vollständig automatisierten Rollformprozess, deren Untersuchung hinsichtlich Drapierbarkeit und Kompaktierbarkeit sowie die Konstruktion eines dafür geeigneten Werkzeuges. Ziel ist die qualitative Bewertung der Proben hinsichtlich form- und prozessbedingter Einflüsse auf die Maßhaltigkeit und Fehlerfreiheit der endgültigen Bauteile.

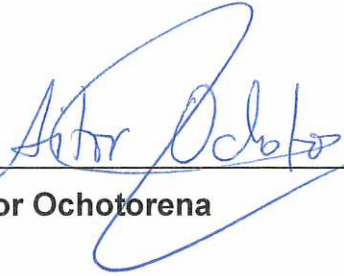
Arbeitsschritte:

1. Literaturrecherche zum Stand der Technik bezüglich der manuellen sowie automatisierten Fertigung mehrteiliger Trockenfaser-Preformen
2. Konzeption eines vereinfachten Versuchsstandes zur Realisierung der relevanten Geometriemerkmale für die manuelle Probenfertigung
 - a. Konstruktion eines formgebenden Werkzeuges für Drapier- und Kompaktierversuche
 - b. Ableiten von Zeichnungen für die Fertigung sowie Beauftragung von Lieferanten
 - c. Fertigung des Werkzeuges
3. Fertigung und Untersuchung von mehrteiligen Trockenfaser-Preformen
 - a. Identifikation von Fertigungseinflüssen auf einzelne Probenmerkmale
 - b. Herausstellen von Empfehlungen für die kontinuierliche Fertigung
4. Anwendung der Erkenntnisse und Fertigung weiterer Preformen für den Einsatz im kontinuierlichen Prozess
5. Schritthaltende Dokumentation der Ergebnisse

Die Studienarbeit wird im Institut für Faserverbundleichtbau und Adaptronik des Deutschen Zentrums für Luft- und Raumfahrt durchgeführt. Die Betreuung seitens des DLR übernimmt Herr Alfred Tempel. Herr M.Sc. Patrick Scholle. übernimmt die Betreuung seitens des IAF.

Änderungen der Aufgabenstellung sind nur mit Zustimmung des IAF möglich. Die Studienarbeit ist fristgemäß elektronisch im WISA-Portal und gebunden in doppelter Ausfertigung im Institut für Adaptronik und Funktionsintegration der TU Braunschweig einzureichen.

Hiermit bestätige ich den Empfang der Aufgabenstellung:

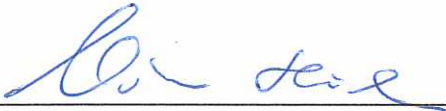


Aitor Ochotorena

Bearbeitungszeit: 3 Monate

Ausgegeben am: 24.01.18

Abgegeben am:



Prof. Dr.-Ing. Christian Hühne

Von: <pdv-fmb@tu-braunschweig.de>
Betreff: Bestätigung des Hochladevorgangs
Datum: Di, 15.Mai 2018 00:53:02
An: <a.ochotorena-esparcia@tu-braunschweig.de>



Sehr geehrter Herr Ochotorena Esparcia,

Sie haben für den Masterstudiengang Luft- und Raumfahrttechnik Ihre Studienarbeit mit dem Titel **Fertigung, Untersuchung und Bewertung von mehrteiligen Preformen** am 15.05.2018 um 00:52:54 hochgeladen.

Erstprüfer ist Prof. Dr.-Ing. Christian Hühne

Ihre Fakultät für Maschinenbau

TU-Braunschweig
Fakultät für Maschinenbau
WISA Online
WISA-Online-fmb@tu-braunschweig.de



Erklärung

Hiermit erkläre ich, Aitor Alejandro Ochotorena Esparcia, geb. am 30.03.1994, die vorliegende Studienarbeit selbstständig und ohne fremde Hilfe verfasst und keine anderen als die angegebenen Hilfsmittel verwendet zu haben.

Braunschweig, den May 15, 2018

Aitor Alejandro Ochotorena Esparcia

Acknowledgements

The present work was created in the context of my master studies at the TU Braunschweig.

I would like to use the first pages of my work to thank all the staff involved in this project for their support and understanding.

Special thanks to my supervisor Mr. Alfred Tempel M.Sc for his useful advice and patience with me during the creation of this work. The regular meetings as well as the mails interchanged were very helpful for the completion of this work.

My thanks also go to Prof. Dr.-Ing. Christian Hühne for letting me hand over my work later than planned.

I am pleased with the basic knowledge I acquired during the realization of this project and I am sure I can take advantage of such experience in future performing projects.

Overview

The intention of this work is to study the quality of the preforms manufactured manually. These preforms will be analysed using parameters such as drapability and compaction, among others. Changing different factors that intervene in the production, like the form of the heat applied or the conditions of pressure and temperature, different results will be obtained. The main goal of this project is to draw conclusions about the main factors that have influence on the final quality of the preforms. For that purpose, preforms with defined geometry of Non-Crimp Fabric (NCF) will be heated by conduction or infrared emissions to achieve a strong activation. Future improvements and guidelines will be deduced from these studies.

Contents

List of abbreviations	xvii
Nomenclature	xviii
1. Introduction	1
1.1. Motivation	1
1.2. Challenge and goals of this work	2
1.3. Methods	2
2. State of the art	5
2.1. Basics of CFRP products	5
2.2. Production of CFRP components	7
2.3. Overview of fiber preforming	9
2.4. Manufacturing process for the production of preforms in Liquid Composite Molding (LCM)	10
2.4.1. Sequential preforming	11
3. Multi-layer preforming - concepts and implementation	13
3.1. Components to be considered	13
3.2. Tooling design	16
3.3. Stacking sequence	18
3.4. Application of heat and pressure	18
4. Production of multi-layer preforms	21
4.1. Fins	21
4.2. L-Fin	23
4.3. C-Fin	24
5. Analysis of multi-layer preforms	27

6. Evaluation of multi-layer preforms	31
6.1. Thickness	31
6.2. Stiffness	38
6.3. Length	39
6.4. Optical analysis	42
6.5. Summary of the quality test	44
7. Summary and outlook	47
List of Figures	49
List of Tables	51
Bibliography	53
A. Appendix	57
A.1. Technical data sheets	57
A.1.1. Dry Reinforcements Woven Fabric	57
A.1.2. Infrared heater	61
A.1.3. Vacuum pump	62
A.1.4. Digital barometer	63
A.1.5. Thermal camera	64
A.2. Stacking sequence woven fabrics	65
A.3. Temperature measurements and data about the heating conditions	66
A.4. ANSYS Simulation: Heat distribution along the fin	67

List of Abbreviations

CAD	Computer-Aided Design
CFRP	Carbon Fibre Reinforced Plastic
DLR	Deutsches Zentrum für Luft- und Raumfahrt e.V.
FWD	Forward
FRP	Fibre Reinforced Plastic
LCM	Liquid Composite Molding
Max.	Maximum
Min.	Minimum
NCF	Non-Crimp Fabric
RTM	Resin Transfer Molding
UD	Unidirectional

Nomenclature

Latin notations

d	Lateral separation between infrared emitters
h	Vertical distance from the infrared source to the preform
z	Longitudinal separation between two infrared emitters
t_{CAD}	Thickness of the part extracted from the CAD reference or desired thickness
t_{MAT}	Thickness of a ply of material
T	Temperature

Greek notations

Δ	Variation
σ	Standard deviation

1 Introduction

1.1. Motivation

According to reports, the future of lightweight construction with textile-reinforced composites looks promising and part of this success is based on the opportunities that carbon fiber is having in aerospace, sporting goods and industrial applications. The demand for carbon fiber in end-use industries together with its breakthrough in commercial aircraft, like B787 and A380, automotive applications and others is leading to the development of new products and energy-efficient structures [1].

The growth of significance that carbon fiber is gaining inside the industrial market is also due to its great properties compared to metals. A higher strength-to-density ratio, an improved deflection resistance and a low heat conductivity are some of the main qualities for which this material stands out [2, p. 1]. These features are essential requirements for aircraft materials to resist the different mechanical stresses found in various flight circumstances [3, 2].

The advances of composites in the aeronautical sector can be observed in the use of this material in the new models of aircraft. Whereas Boeing has had to make a large jump from 10% composites in the B777 airliner to the B787's 50%, Airbus has progressively adapted fairings, nacelles, empennages and wings to its composite portfolio [1, p. 1].

At the same time, other factors like the increase of flights in the last years as well as the need to save fuel have led to focus more on the optimization of the aircraft materials and reducing weight is, in fact, one of the priorities for the aircraft manufacturers. For that purpose, Carbon Fibre Reinforced Plastic (CFRP) presents itself as a viable alternative due to its low weight in comparison to metals [4].

Regarding the automated production of CFRP components, several manufacturing processes can be found but one of the most important is the Resin Transfer Molding (RTM) process consisting of different stages. The key steps here are the preforming process and the injection. Dry fiber material adopts a shape and is fixed before the resin is injected (preform).

Subsequently, the preform is placed by hand or by a robot in a mold where resin is

infiltrated in the injection process and the component is cured. Automated processes permit costs reductions, making preforming more efficient. Thus, a combination of automation and handling to form a total preform enables an increase in the quality of production [5].

1.2. Challenge and goals of this work

One of the aims of the Institute of Composite Structures and Adaptive Systems in the Deutsches Zentrum für Luft- und Raumfahrt e.V. (DLR) is to accelerate the development of an automated preforming concept, manufacturing and joining process in end-line assembly, contributing to a reduction in overall cost and throughput times.

In cooperation with an aircraft manufacturer, high-rate production of CFRP components is being developed, permitting new possibilities for close-to production. Within the work package, C-profile beam preforms are to be automated and continuously manufactured, whereby additionally, the prepared and provided load introduction fin is integrated during the process between these two C-profile beam preforms.

Mainly this work seeks to study the quality of the manufactured preforms done by hand. The important issue here will be to find out which factors have influence on the final quality of the preform in order to justify the obtained results and improve future tests. Special consideration will be given to the design of an adequate tool that shapes the C-profile beam preforms and their reinforcements in their final shape.

Finally, with this work it is expected to acquire a wide view on the preforming technologies and Fibre Reinforced Plastic (FRP) processes. The quality requirements involved and techniques applied will help the reader to assess the quality of the process.

1.3. Methods

In this work, a qualitative evaluation of the resulting multilayer preforms and their reinforcements with regard to shape, compactness and visual quality will be conducted. For this evaluation, some of the aspects that play an important role in the final component are shown in the following figure:

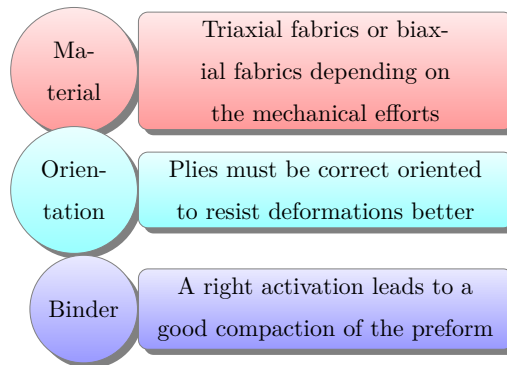


Figure 1.1.: Factors of influence on the quality of the preform

The orientation of the material, the number of plies, the conditions of pressure and temperature or the time of heat applications have to be taken into account to achieve an optimal product. In this work three parts can be differentiated:

- A theoretical part : in chapter 2, that gives an overview of the nature of the CFRP and its manufacturing processes.
- A descriptive part : where the materials and techniques used (chapter 3), as well as the development of the manufacture of preforms will be discussed (chapter 4).
- An analytical part: : in chapter 5 and chapter 6, in which the quality of the pieces obtained will be evaluated as well as the reasons for these results.

The manufactured preforms in this document are used for investigations issues in the field of component quality, process reliability and the validation of new production concepts. The infusion of the preforms into completely structurally resilient components is not included in the scope of this project.

2 State of the art

Both properties of the starting material and the manufacturing processes exert a big influence on the final component. This will be explained in the following sections.

2.1. Basics of CFRP products

In the production of CFRP components the fusion of carbon fibers and a matrix result in a fiber-reinforced plastic composite, obtaining an “increase in the strength in the base material” according to Schurmann [6].

Mechanically, the fibres of the CFRP take over most of the mechanical loads in a composite, while the matrix stabilizes it. In Table 2.1, the main functions of the fibers and the matrix are summarized [7, 8]:

Matrix	Fibers	Composites
<ul style="list-style-type: none">• Provide stability to the whole by transferring the loads to the reinforcement• Protect the reinforcement against mechanical and chemical deterioration• Avoid the propagation of cracks• Maintain the composite structure aligning the carbon fibres	<ul style="list-style-type: none">• Provide the required tensile strength• Provide rigidity (high elastic modulus)• Conductivity or electrical insulation depending on the type of fibres.	<ul style="list-style-type: none">• High strength to weight ratio• Lightweight• Design flexibility• Low thermal conductivity

Table 2.1.: Properties of matrix, fibers and as a composite [9]

Properties of fiber composite depend on other key factors, like the fiber orientation, fiber volume content, number of plies or the rate of compaction by preforming, among others [10].

Regarding types of semi-finished carbon-fibers, Unidirectional (UD) rovings and woven fabrics can be found [11] but this work is focused on the application of multi-axial NCF.

- Multiaxial NCF:** consist of one or several layers of long fibres, which are held by a secondary binder. They can resist multiple stresses due to the multiple orientation of the layers. The layer layup can be done in a different order, resulting in different mechanical properties. The stitching process allows a variety of fibre angles. Typical angle values to be combined into one fabric are 0° , $\pm 45^\circ$, 90° , as shown in Figure 2.1.

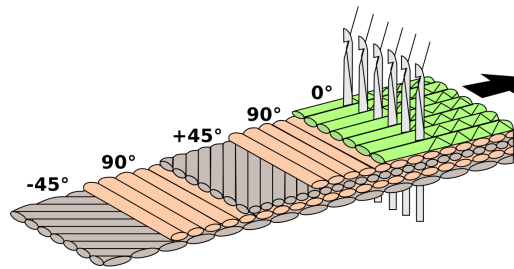


Figure 2.1.: NCF layout [12]

Multiaxial fabrics used in this work are biaxial (Figure 2.2) with two or three layers of carbon fiber and an incorporated layer of toughener between every two layers. The main parameters of the NCF fabrics used are found in Appendix A.1.1 .

Sewing thread starts at a temperature around 160°C to decompose. Therefore, a surface temperature above 160° will be avoided during the execution of the experiments. The activation of the binder will take place at a temperature around $100^\circ\text{-}130^\circ\text{C}$ [13].

The orientation in the carbon fabric provides superior characteristics to most metals and other reinforced compounds, providing the ability to create resistant and lightweight designs[14, 15].

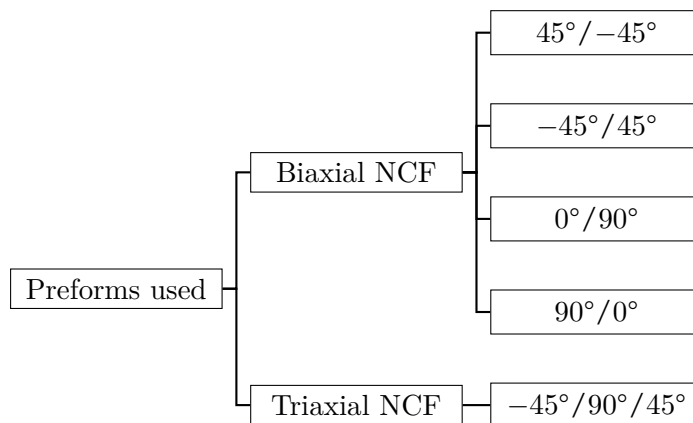


Figure 2.2.: NCF used and orientations

2.2. Production of CFRP components

In the production of composite materials, the manufacturing processes can be very different depending on the geometry and complexity of the final component. An overview of the most relevant ones according to the geometry and complexity of the part is shown in Figure 2.3

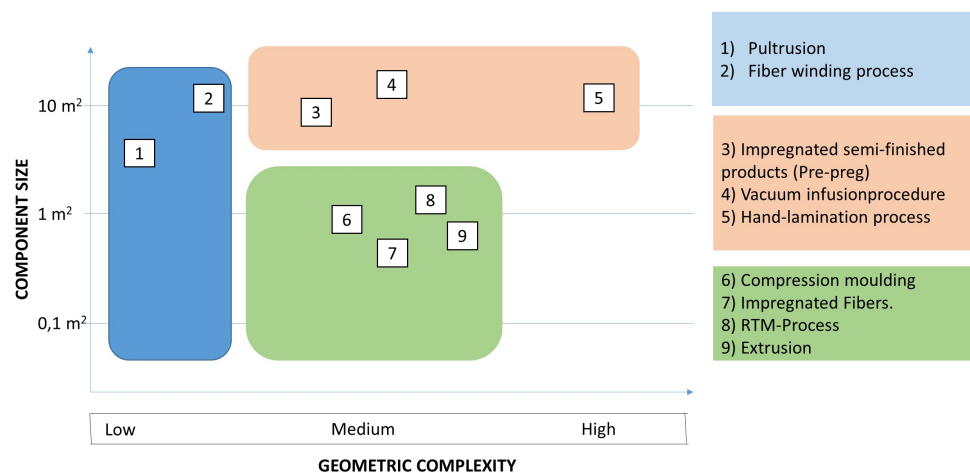


Figure 2.3.: Main production processes based on the component geometry [16, p. 13]

Among all these processes, the focus of this project lays on the study of the preforming for RTM, so the other procedures will not be under consideration for now.

In RTM processes, both fibers and resin can be directly combined (like in winding processes) or semi-finished products are applied using appropriate textile techniques, such as weaving, knitting, etc. and then impregnated with resin at the end of the process chain [17].

To illustrate how the steps of the manufacturing process can vary until the final component, Figure 2.4 shows the process chain where fibers and resin turn into a final product.

According to Schmalz et al. [18], in the first step of RTM manufacturing process, the shapes are cut from the supplied rolls. These cut shapes are placed in a defined order to create a layer structure and depending on the process, the pieces are heated or automatically draped to create a preform. In section 2.3, the importance of the preforming process will be discussed. After preforming, the preform is closed inside a RTM press.

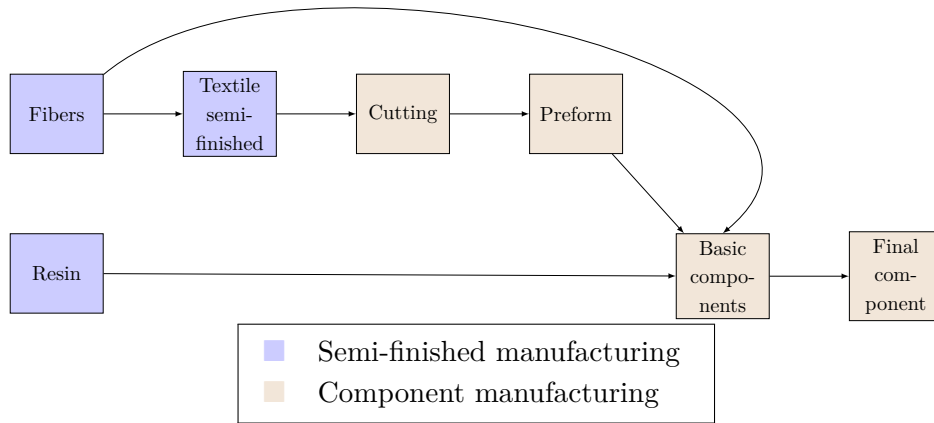


Figure 2.4.: Value chain of continuous fiber reinforced composites [17, p. 47]

A resin and a hardener are injected into the cavity. Once the workpiece is finished, the RTM press is opened again and the shell component is removed and fed to the final processing. Usually a finishing process, such as milling or water jet cutting, takes place [18, 17]. The flow chart of the respective RTM process is displayed in Figure 2.5 . Typical applications include automotive, rail and aircraft components with relatively complex geometry.

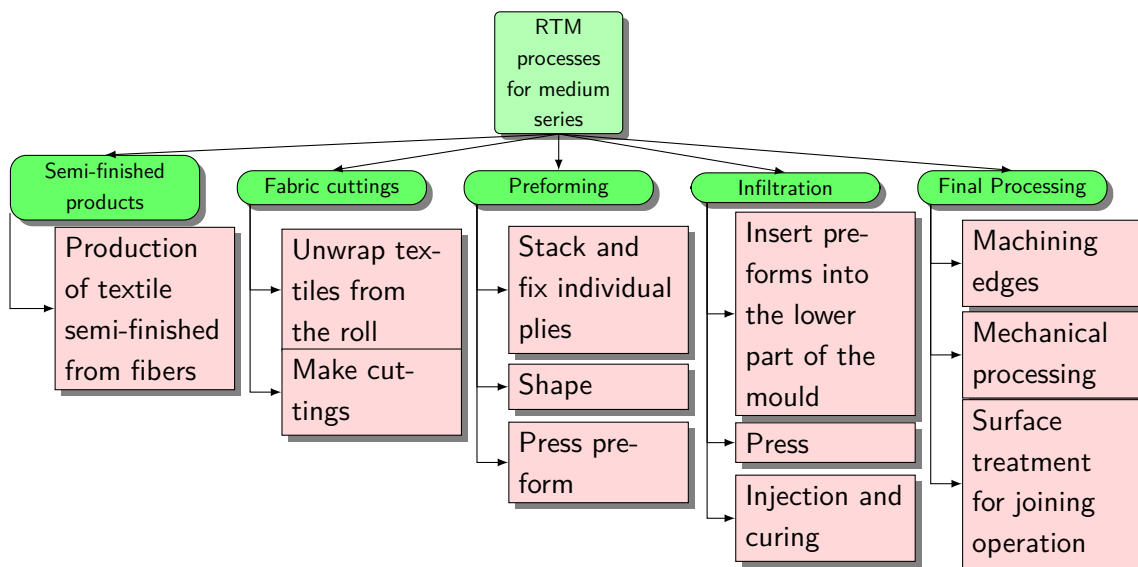


Figure 2.5.: RTM process for medium series[17, p. 13]

2.3. Overview of fiber preforming

The fiber preforming process is a crucial step for the shape of the final component. According to Kruckenberg et al. [19], during the fiber assembly in the RTM process, many layers are first brought together as a roving or a tow acquiring the shape of the finished part. The preforming process converts the fiber reinforcement, also known as preform, into the part geometry. Typical preforms include bidirectional and triaxial fabrics and other combinations of stitching, weaving, braiding, etc. Apart from the mechanical properties, Kruckenberg [19] states that two attributes characterize a fiber reinforcement, such as the bulk factor, or the ratio of volume between compacted and non-compacted part, and the drapability, or the quality to conform the contours of a mold cavity.

In this work, during the production of the preforms, one can realize that one of the challenges that the preforming technique presents is the preforming stage. Layers must be cut and shaped to the tooling surfaces, which is a time-consuming process. In addition, the fibers may move during the application of pressure and additional fasteners are required to fix the part in a position. In a close mold it can be even more complicated to fix the preform while pressure is being applied.

Moreover, parts with complicated geometries are difficult to give them shape and different defects could appear. Stretching causes thinning, bending results in springback and in-plane compressions causes wrinkles, which is undesirable as dimensional changes could take place and the component may not match in the mold cavity[19].

According to Nezami [20], in multiaxial fabrics, rovings can move freely in the individual layers by the knitting threads or loops . If the deformation force exceeds the strength of the fixing threads, then they break and allow a free movement of the rovings. However, the movements are influenced by the interwoven architecture of warp and weft threads, significantly more obstructed than in unidirectional semi-finished products. Shear stresses are here the most dominant deformation [20]. How fibers deform along the surface can be illustrated in Figure 2.6

In section 2.4, the focus will be set on the developed technologies for preforming processes.

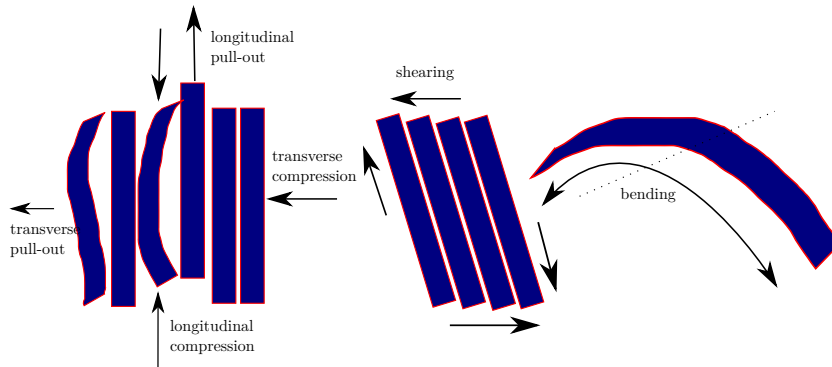


Figure 2.6.: Deformation mechanisms of textile semi-finished products [20, p. 22]

2.4. Manufacturing process for the production of preforms in LCM

In the production of preforms, a distinction is made regarding to the complexity of the part between direct and sequential preforming. Preforming processes can be subdivided into direct and sequential preforming and can be seen in Figure 2.7.

Those processes, that shape the desired geometry of the preform in one step, are direct preforming processes [21]. By sequential preforming, draping a fabric takes place after cutting. The technology used for this project is based on the sequential preforming and in the next parts, this issue will be addressed.

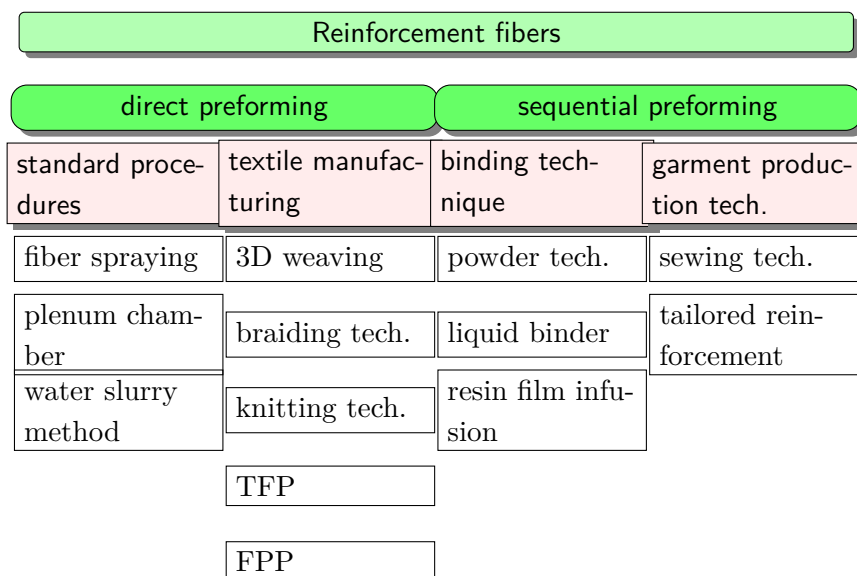


Figure 2.7.: Preform technologies[21, p. 31]

2.4.1. Sequential preforming

In this work, binder systems are used. These systems are activated under the action of heat, forming a manageable preform. Depending on the type of procedure, the peel test or cantilever test will be applied to study the stiffness of the preform, i.e. the binder distribution in the preform can be estimated by measuring the deflection of the preform under a certain load. The activation of the binder depends on certain aspects, like the geometry of the preform, the placement of the heating radiators, the power of irradiation or the thickness of the component [22].

The use of powder binder systems is suitable for NCF and woven fabrics, as well as for short fiber preforms. The powdered binder must be sprinkled onto the reinforcing fibers and melted or thermally activated [23].

3 Multi-layer preforming - concepts and implementation

In this chapter, the conditions for the construction of the final components will be described. A series of pieces of different geometries are printed like flattened geometries as stencils and they will be molded acquiring the shape of the tool. As mentioned in chapter 1, the main focus lays on a study of quality, reliability of the process and the validation of new concepts. The application of heat permits the activation of the binder, whereas the force applied in the material gives it its shape.

3.1. Components to be considered

The C-profile preforms and the load introduction fin to be manufactured and integrated are derived from beams for CFK flaps. After the spars have been formed they are joined together with other spars and the skin to form an integral flap preform. [24].

These parts have been designed looking for a balance between a light design, a gradual reduction of the thickness of the layers for a better adhesion and a low potential for initiation of fractures [13]. The manufacturing is reduced by creating different pieces. The final assembly of all the components is shown in the Figure 3.1:

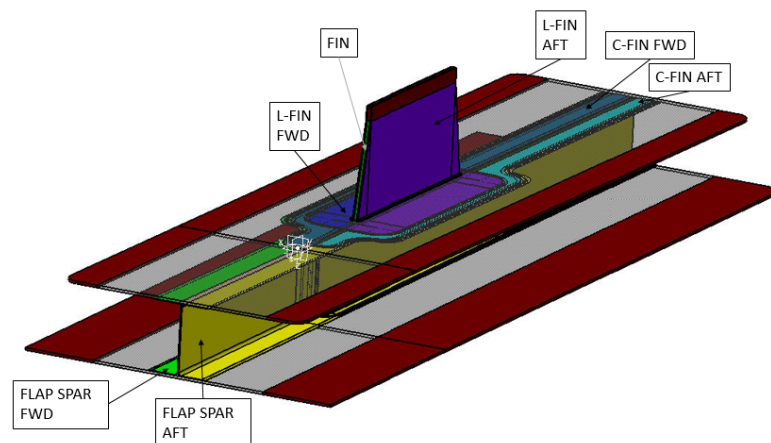


Figure 3.1.: Assembly of all components [13, p. 5]

Beam preforms/ Flap spars

Beam preforms are part of the components that integrate this project. These parts are more elongated than the rest of the pieces and will resist higher mechanical stresses. There are two designs (FLAR SPAR AFT and FLAP SPAR Forward (FWD)). Within the overall assembly, the double C-profile spars are load-bearing components and provide a load introduction to the integrated fins. These parts are provided by the aircraft manufacturer and will not be manufactured during this work.

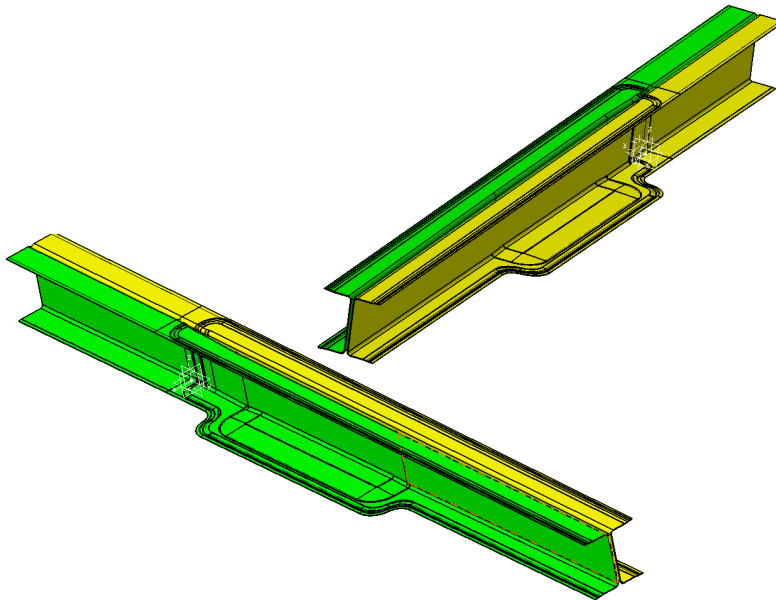


Figure 3.2.: Flap spars solids

Load initiation fins

This flat component is formed by five different geometries, which are stacked one over another. The CAD-reference keeps a gradual variation of thickness, simplifying the design of the model. Figure 3.3 shows the flattened geometries, which will be repeated to form the shape of the fin.

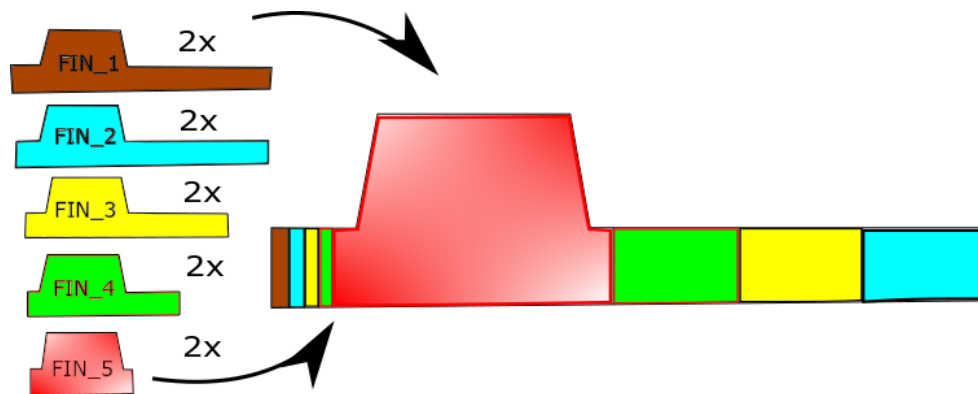


Figure 3.3.: Base geometries and final layout of the fin

Each geometry is repeated twice. Only biaxial materials will be used here for the fin and indeed ten biax fabrics will be used, in total 20 plies of material, alternating orientations of $+45^\circ / -45^\circ$ and $0^\circ / 90^\circ$. In the design of the chosen fin concepts, the scope is to design sub-preforms "from the inside out" forming a final component.

This part does not present any curvature and therefore, no additional tooling is required to make its shape. However, the difficulty of this part is the activation of so many plies of material. Here, because there are so many plies of material, special attention must be paid to the application of heat. If the preform is not heated enough, plies can be detached and if it is overheated, fibers may be damaged.

L-Fin

This symmetrical part is repeated on both sides of the fin (L-FIN AFT and L-FIN FWD). In this component, the thickness is constant throughout the preform and therefore, the geometries of which the total piece is composed are repeated for the construction of the piece.

Through the L-Fins, the load can be better distributed at the fin and failures such as delamination or fiber pull-out can be reduced. In this part an additional tooling has to be designed to give shape and an iron is used to activate the binder, as it is the easiest way to shape a curvature.

Reinforcing plies/ C-Fin

Reinforcement plies are used to provide the fin with better stability and structurality. These parts are made of dry CFRP material and constitute part of the total preform.[25]. Like the L-Fins, these parts are preformed on a tool with an iron to give the shape. They distribute the load into the flap spar. These parts are easier to be preformed than

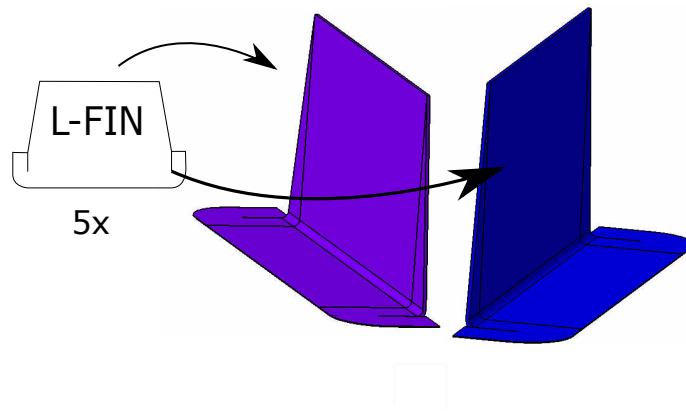


Figure 3.4.: Base geometries and final layout of the L-fin

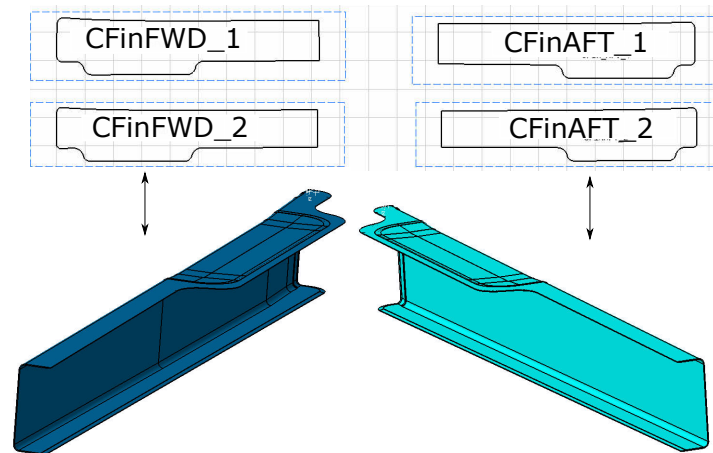


Figure 3.5.: Base geometries and final layout of the C-fin

the others because they have only two layers of material.

3.2. Tooling design

The tooling has its importance to give the shape to the preform. For that purpose, a tool composed of four separate solid aluminum cores is provided by an aircraft manufacturer. Pressing force of vacuum tightens core assembly and on the backs of the aluminum cores, there are grooves on the surface for infiltration of the resin. However, with this tooling it is difficult to reach a high temperature in the lower layers of the preform, because the tooling is robust and needs long time to be heated. Besides, the robustness of the cores hinders a good maneuverability.

Instead, an aluminum plate will be bent according to the measurements that the preforms need. In Figure 3.6 the details of both toolings can be seen:

At the beginning, a design of a tool with the shape of the C-Fin was thought as it

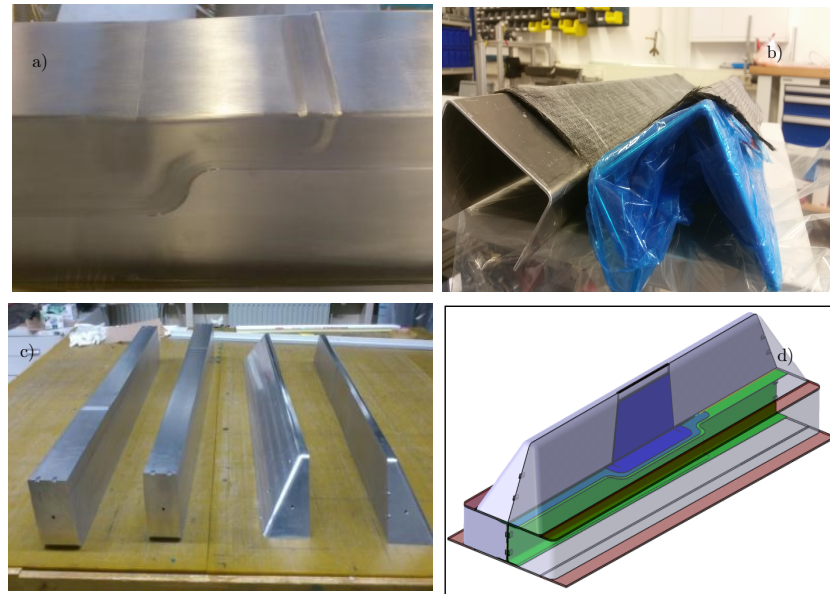


Figure 3.6.: Details of the tooling: a) Grooves on the lower cores; b) Aluminium plate folded; c) Cores of the tool; d) Assembly of the cores and the part together.

would be more accurate if the geometry is directly extracted from the negative shape of the CAD files. However, the complexity of creating a metal tooling for this test, led to opt for giving shape to the aluminium plate. The measurements for the shape of the aluminium sheet are summed up in the Table 3.1:

	C-Fin Aft (mm)	C-Fin Fwd (mm)	L-Fin (mm)
Length of the part	905	925	350
Minimum and maximum height of the web	83.97/93.11	83.97/93.11	129.5
Minimum and maximum width of the flanges	32/78	34.5/78	62
Radius at the transition web/flanges	5	5	4

Table 3.1.: Geometrical measurements for the aluminium sheet

For the fin form no additional tooling is needed, since it is flat and does not require a special tool to make the shape of its curves. However, a support for the infrared emitters will be built to heat the fin (Figure 3.7).

When folding the aluminum sheet to get 90° in the transitional arc between the web and the flanges it is important to take into account the recoil forces, that act on the material tending to stabilize the piece after being bent. For that reason, the aluminium blade will be bent $2\text{-}3^\circ$ more in order to get 90° in the final preform part.

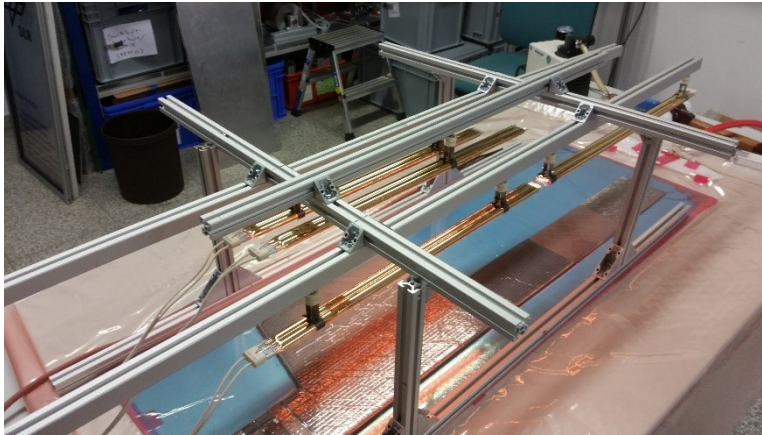


Figure 3.7.: Support for infrared emitters

3.3. Stacking sequence

The sequence of the layers is included in Appendix A.2. The proposed orientation of the plies seeks to enhance the mechanical properties of the material and avoid finishing defects.

3.4. Application of heat and pressure

To achieve a preform, both heat and pressure are needed to be applied simultaneously. Depending on the geometry of the piece, the method of heat transfer is chosen. Each method offers its strengths and weaknesses.

By heat conduction, ironing is used to activate the binder, while by radiation, infrared emitters can be used.

Generally, radiation is preferred to be applied when the component does not present many difficulties in the geometry, because the application of radiators involves the construction of a support, which can be too cumbersome for what is needed.

The use of infrared emitters is in general, faster and more powerful than the use of ironing (1500 W of the infrared emitters [Appendix A.1.2] against the 1200 W of the iron [26]).

Besides, very good finishing conditions can be achieved by radiation, as the heat source does not interact directly with the material and if the emitters are properly distributed, the heat distribution can be very favourable achieving a good degree of compaction. An additional ironing could be included for positions that were not activated properly.

On the other hand, ironing allows to activate difficult positions of the preform, as edges

Name	Form of heat application
Fin A	Radiation
Fin B	Radiation
Fin C	Radiation
Fin D	Radiation
L-Fin 1	Conduction
L-Fin 2	Conduction + Radiation
C-Fins	Conduction + Radiation

Table 3.2.: Distribution of heat along the different preforms

or curvatures. Although a better compaction along all the surface can be reached using radiation, ironing is an effective way to activate individual positions. In the successive tests, both forms will be applied depending on the geometry.

Concerning pressure, it can be transmitted by the weight of the iron on the surface, but when radiation is applied, an external pressure must be provided, i.e. with the use of a vacuum pump. In Table 3.2, it can be seen, that fins are heated by radiation because they present a flat geometry. L-Fins and C-Fins are heated by conduction and in some parts, radiation is applied at the same time to increase the temperature in the lowest layers.

4 Production of multi-layer preforms

In this chapter, the most relevant aspects and related comments that can be extracted from the manufacturing process of the preforms are described in detail. Changing different aspects, such as the time of heat application or the heat transfer method (ironing or infrared light) different results are obtained.

4.1. Fins

'Preform' implies pressure and heat at the same time. For the manufacturing of flat geometries, infrared emitters (Appendix A.1.2) as a heat source will be applied and to subject the part into pressure, the air between the plies will be extracted through a vacuum pump (Appendix A.1.3). In these tests, an adequate pressure between 400-550 mBar is tried to be reached and the distribution of the infrared emitters will be carefully considered.

In the manufacture of fin A, the heat application consists of two steps. In a first step the fin is heated by the infrared emitters during 40 minutes at 40% power at a distance of 220 mm until 120°C is reached in any position. Afterwards, positions, whose temperature are below 120-130°C, will be heated until they reach these values. 25 additional minutes of radiation at 60% power were applied, trying to prevent the overheating of fibers. An adequate application of heat, checking that the temperatures are not surpassed, strongly influences the activation of the binder in all layers and as it will be shown later, creating stability and stiffness.

In Figure 4.1b the heat distribution of the fin is shown and their values are gathered in Appendix A.3.

In the manufacture of the following fins, following parameters are varied to prove their influence on the final results.

1. Time of heat application

In fin B, the guidelines of the manufacturer are followed (subsubsection A.1.1) and 120°C are applied on the surface during 20 minutes on the surface, obtaining the following shape (Figure 4.2). As will be explained later, all layers are fixed but a longer heat application would result in a greater stiffness.

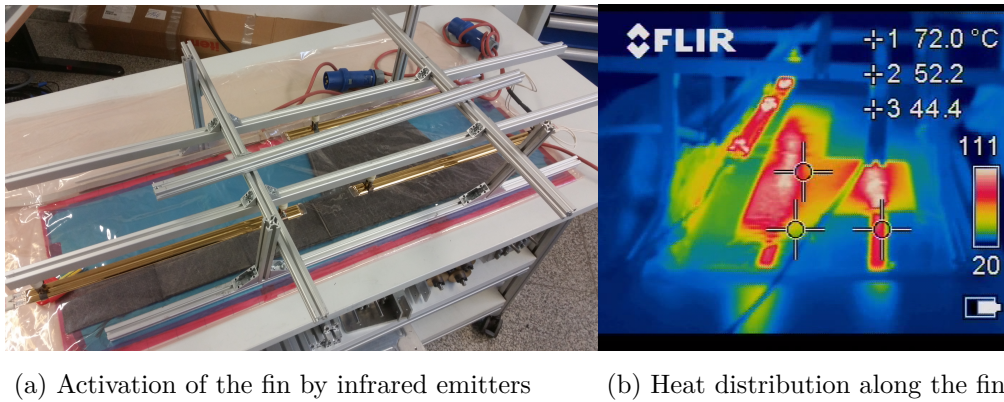


Figure 4.1.: Activation of plies in the fin and thermal distribution

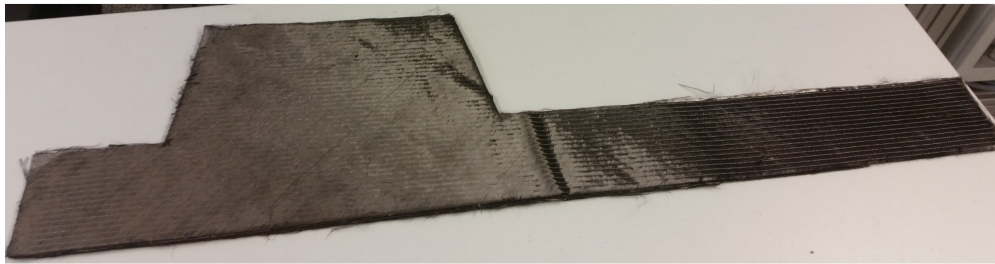


Figure 4.2.: Final shape of fin B

2. Position of the heat emitters

In fin C, the distance between radiators was increased from 5 mm to 9 mm and as a result, a wrinkle was formed. Wrinkles occur because the ends of the material are activated but the air in the middle between the plies gets trapped. An inadequate position of the heat emitters influence the final result.



Figure 4.3.: Final shape of fin C

3. Conditions of pressure or temperature by preforming

In fin D a lower vacuum pressure was obtained because the same bag as in the

third test was reused and a wrinkle appeared as a result. Besides, this fin is not very compacted.

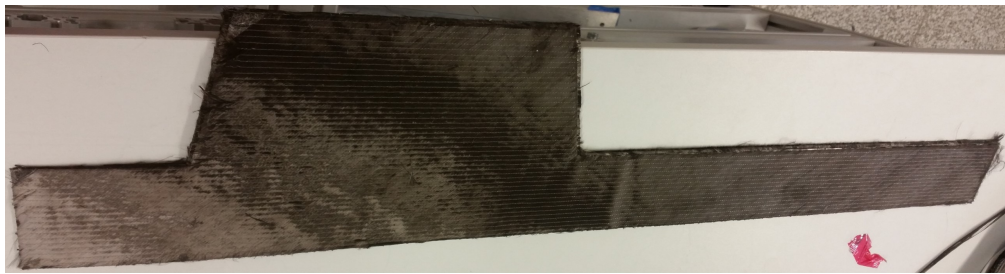


Figure 4.4.: Final shape of fin D

4.2. L-Fin

For this geometry, manual heating will be used for the preform, because there is a curvature in the design of the part. Several molds can be used to form a L-Fin : the tooling provided by the aircraft manufacturer or an aluminum sheet with the shape of the L-Fin.

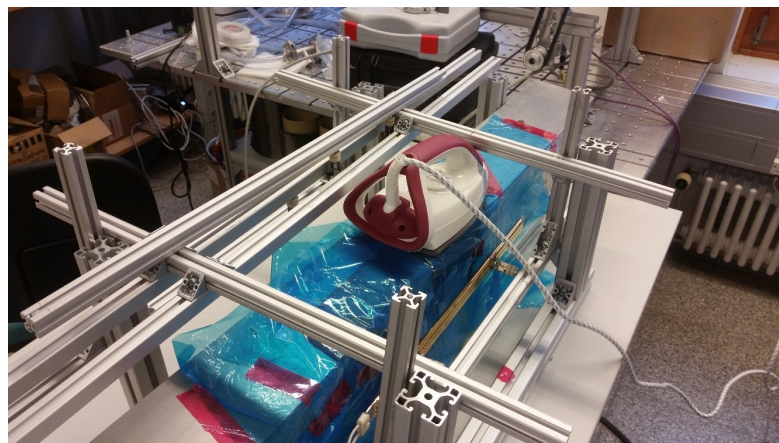


Figure 4.5.: Heat application on the L-fin 1 by means of an iron. An infrared emitter warms the surface of the tooling to promote the activation of the plies

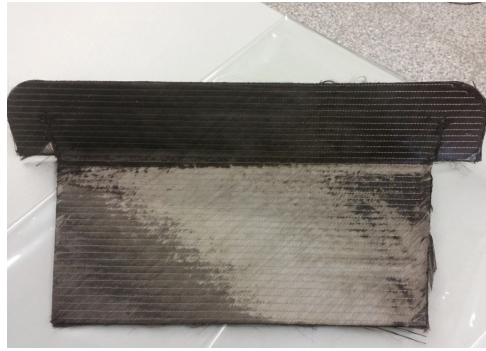
The first L-Fin, compacted from the aircraft manufacturer's tooling, has a rough finish quality on the borders because the preform is inserted into a cavity and the contact with the tooling makes fibers loose. In addition, the application of heat along the edges is more complex.

L-Fin 2, on the contrary, was shaped on the aluminium plate. The desired temperature can be easier achieved through the use of an iron and infrared emitters. They just warm

the surface to promote the activation of the binder (Figure 4.5). Although the quality increases, displacement between layers can occur causing deviations with the desired lengths.



(a) L-Fin 1



(b) L-Fin 2

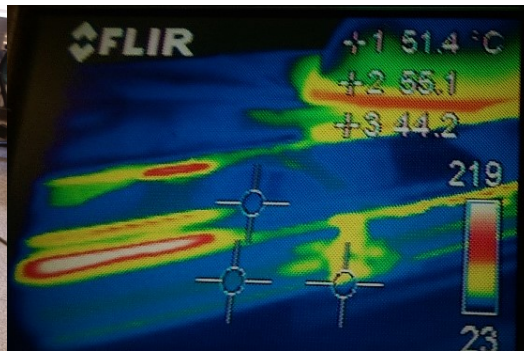
Figure 4.6.: Final shape of the L-Fin

4.3. C-Fin

Here, an iron and an infrared emitter are used to shape the preform. Orientation must be taken into consideration as an incorrect orientation can lead to defects in the preform and a reduction of the mechanical properties of the piece. Activating few plies takes less time than doing it with many plies and the whole surface can be activated.



(a) Heating a C-Fin with iron and infrared emitters



(b) Thermal distribution of C-Fin in the activation of the plies

Figure 4.7.: Activation of plies in C-Fin and thermal distribution



(a) C-Fin AFT



(b) C-Fin FWD

Figure 4.8.: Final shape of the C-Fin

5 Analysis of multi-layer preforms

In this chapter, different quality aspects of the preforms will be tested. The quality requirements applied were extracted by Tempel [25].

The preforms to be produced are not resilient but are dimensional flexible components, i.e. materials experience deformations, even after the processes are done, due to restoring forces or dead weight.

This chapter will describe the main quality deviations that might be found in the preform and which criteria will be used to assess it.

Fraying single fibers

- Description: Visible damages such as pulled out or broken rovings.
- Effects: Mechanical properties and geometry of the preform can be affected.
- Assessment criterion: Folds of material larger than 2 mm from the reference plane are not allowed.

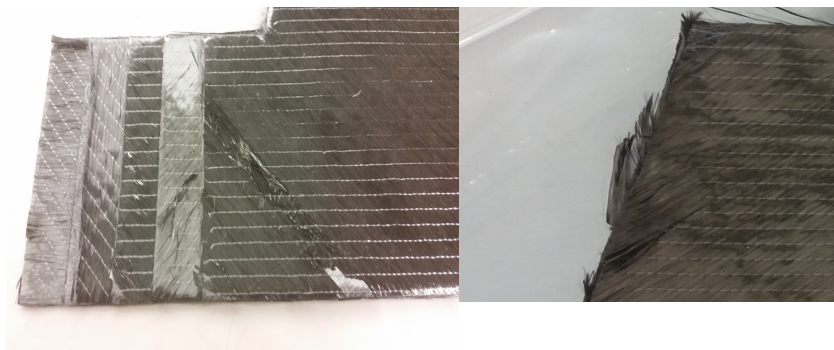


Figure 5.1.: Frayed fibers in the preform

Overheating

- Description: Overheated areas and resulting uplifting of fibers or areas.
- Effects: Mechanical properties and geometry of the preform can be affected.
- Assessment criterion: Uplifting of material larger than 2 mm from the reference plane is not allowed.

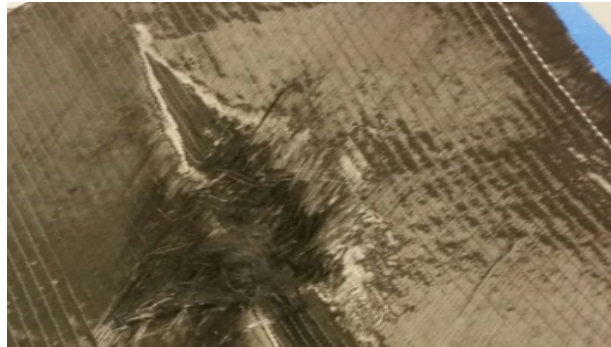


Figure 5.2.: An intensive heating can bring to the detachment of the fibers

Displacement between plies

- Description: Deviation or displacement of the plies from the reference leads to variation in the length measurements.
- Effects: Mechanical properties and geometry of the preform can be affected. Closing of the tool in the subsequent infusion process can be affected as well as a connection with other components.
- Assessment criterion: No deviation more than 2 mm/m is allowed.

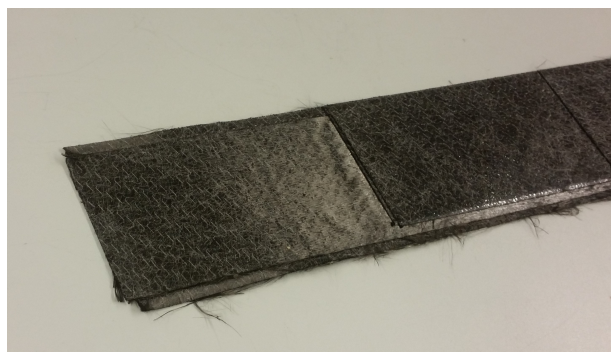


Figure 5.3.: Displacement of the plies in a preform

Wrinkles, waves and gaps between the plies

- Description: Excess of material appears in the component due to an inadequate attachment.
- Effects: Mechanical properties and geometry of the preform can be affected. Closing of the tool in the subsequent infusion process can be affected as well as a connection with other components.

- Assessment criterion: No deviation more than 3 mm is allowed.



Figure 5.4.: Gap and wrinkle found in the preform

Fin thickness

- Description: Deviation of the measured thickness of the fin from the CAD-reference.
- Effects: Deviations out of this margin can prevent the closing of the tool in the subsequent infusion process and affect the mechanical properties.
- Assessment criterion: The fin to be integrated must not deviate more than 10% from the CAD reference in its position at any point.

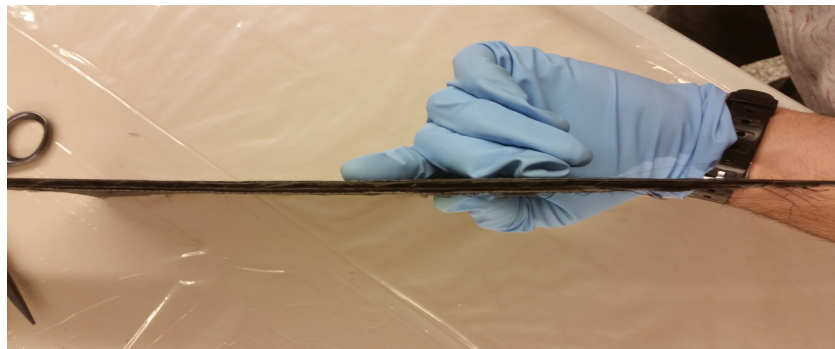


Figure 5.5.: Fin in profile

Angular deviations

- Description: Deviation of angular measurements from the CAD-reference.
- Effects: The shape of the resulting preform and the final mechanical properties of the component might be affected. Any deviation outside the allowed margin will require a spare deformation of the preform to introduce it into the press.

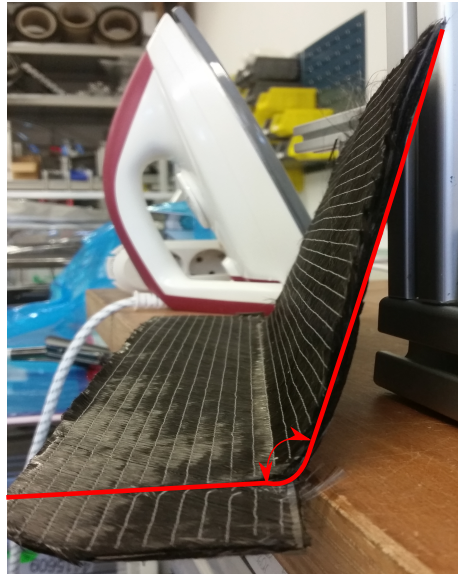


Figure 5.6.: Angle measurement of a L-Fin

- Assessment criterion: Any deviation bigger than 10° is not allowed.

Poor adhesion of plies

- Description: Inadequate stacking of the plies.
- Effects: Mechanical properties and geometry of the preform can be affected. A poor compaction hinders the closing of the tool for the subsequent infusion process.
- Assessment criterion: Visible criterion.



Figure 5.7.: Plies fall out due to an insufficient adhesion

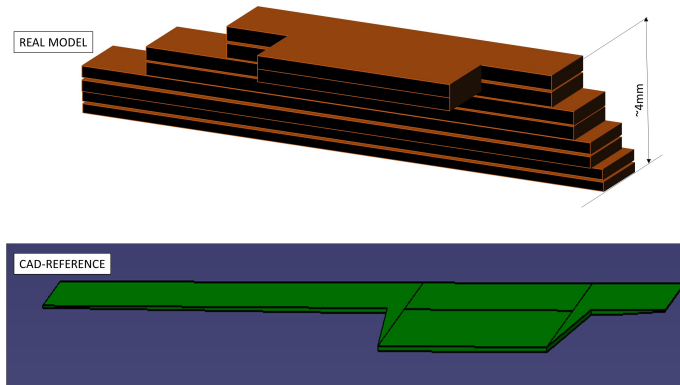
6 Evaluation of multi-layer preforms

To assess the quality of multilayer preforms, this chapter will be focused on the control of several important parameters of the preforms, such as thickness, stiffness and length of the parts. Apart from these measurements, a visual inspection of the preform will be carried out to understand which factors contribute to its final quality. The control of these parameters is crucial, so that the infusion processes can be carried out correctly. Through this analysis, the manufacturing deviations with respect to the original model will be identified. For this purpose, the number of measurements collected and how these are taken exert a big influence on the final result. Conclusions extracted in this analysis may be useful for the improvement of the manual process.

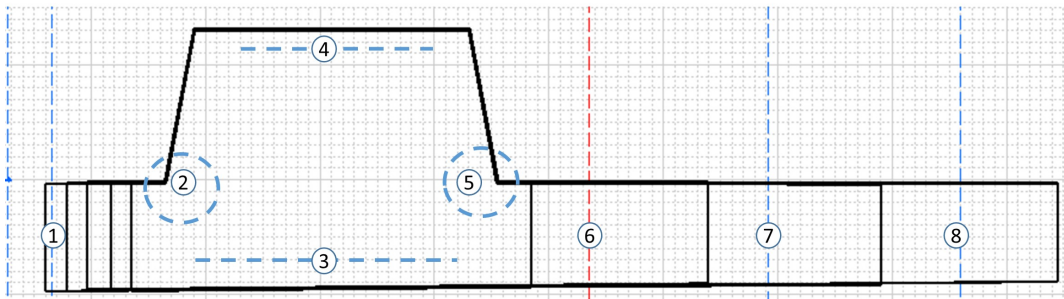
6.1. Thickness

Taking a look at the fin geometry, it can be observed how thickness changes along the component. As will be explained later, the thickness of the part provides interesting information about the compaction of the final piece. By comparing the initial thickness with the one after compacting, important conclusions can be drawn about how the compaction process has been.

In reality the parts have a staged geometry consisting of an arrangement of several plies (see Figure 6.1a). Because the thickness of the fin is unsteady, a set of representative points are chosen in order to check the thickness of the fin in different positions (Figure 6.1b). Every position was measured eight times and the plotted columns of Figure 6.2 show the average thickness of these measurements for every fin. An orange line shows the average thickness for the four fins in every position.



(a) Real model and CAD model



(b) Positions of measurement for the fin

Figure 6.1.: Fin layout and measurement positions

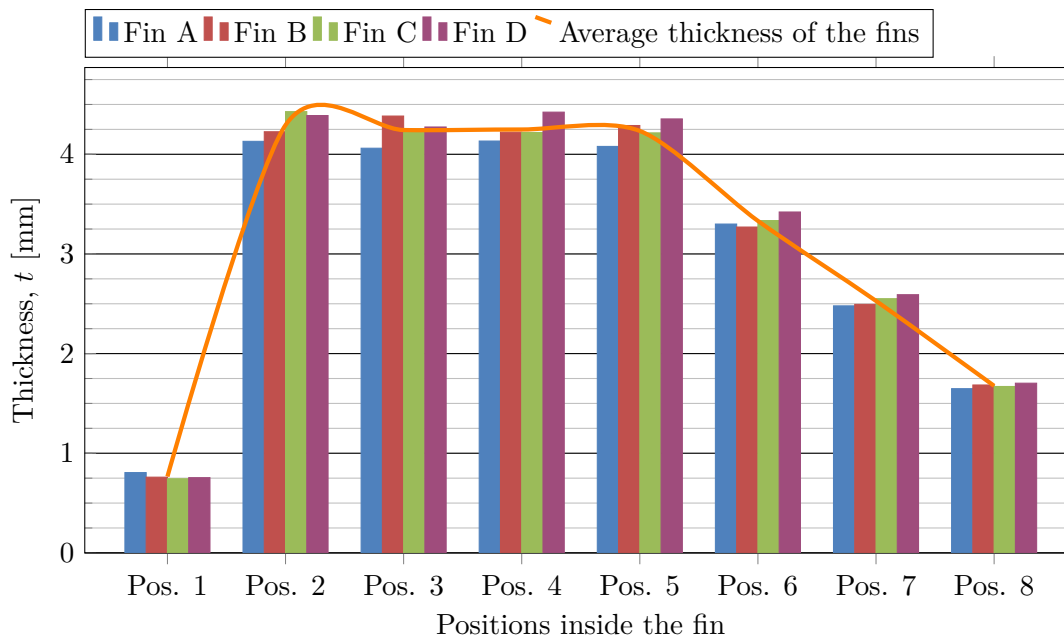


Figure 6.2.: Average thickness of Fin A, Fin B, Fin C and Fin D for the different positions

In Figure 6.2 it can be seen how plies are distributed along the fin, obtaining a larger thickness in the middle positions. There is a larger variation of thickness between the different fins in the middle positions than in the end positions. Results converge, therefore, more in the end positions than in the middle ones. This is due to several reasons:

- First of all, taking measurements in the end points of the fin is not so complicated as taking these from the middle points as there is a higher flexibility to measure points. That could explain why in the Pos. 1 and Pos. 8 more uniform measurements can be found.
- Secondly, as many plies are stacked in the middle positions, compaction cannot be achieved so properly. With fewer layers, it is easier to activate the binder because it is easier to create a vacuum atmosphere.

The deviations of measurements for every position, together with the average thickness of the fins are illustrated in Figure 6.3.

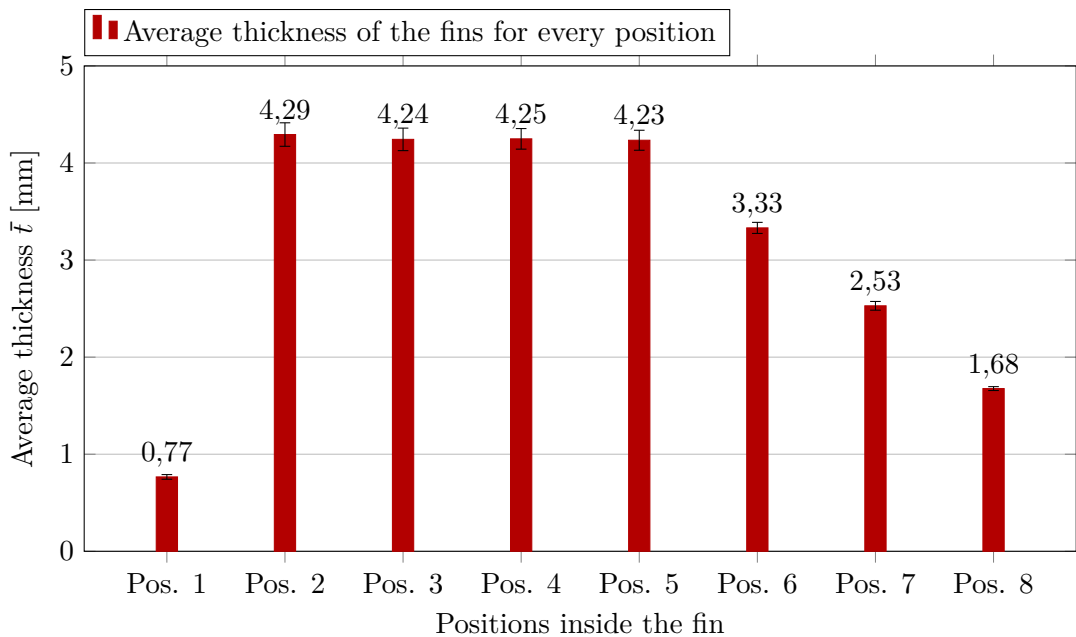


Figure 6.3.: Average thickness of the fin geometry for the different positions

The final thickness of the preform shows how compacted a component is. This can be measured by showing the deviation between the average thickness of the position (\bar{t}) and the desired one given by the Computer-Aided Design (CAD) reference (t_{CAD}). This

value (Δt_{CAD}) is expressed in a percentage form under Equation 6.1:

$$\Delta t_{CAD} = \frac{\bar{t} - t_{CAD}}{t_{CAD}} \times 100 \quad (6.1)$$

Another form to express the compaction can be given by calculating the deviation between the average thickness of the position and the sum of the thickness of every ply separately ($\sum t_{MAT}$). This value (Δt_{MAT}) is expressed in a percentage form under Equation 6.2:

$$\Delta t_{MAT} = \frac{\bar{t} - \sum t_{MAT}}{\sum t_{MAT}} \times 100 \quad (6.2)$$

In Figure 6.4, the deviation of the average thickness with respect to the desired one (that is the CAD reference) is shown. However, the measured thickness of the material varies from the theoretical one. Theoretically, a ply of biax is 0,4 mm thick. Measuring this in reality, a thickness of 0,408 mm has been reached. That is why at some positions, the maximum limit is surpassed. Figure 6.5 shows the deviation between the measured thickness of the preform and the real material and here, the values are within the margin.

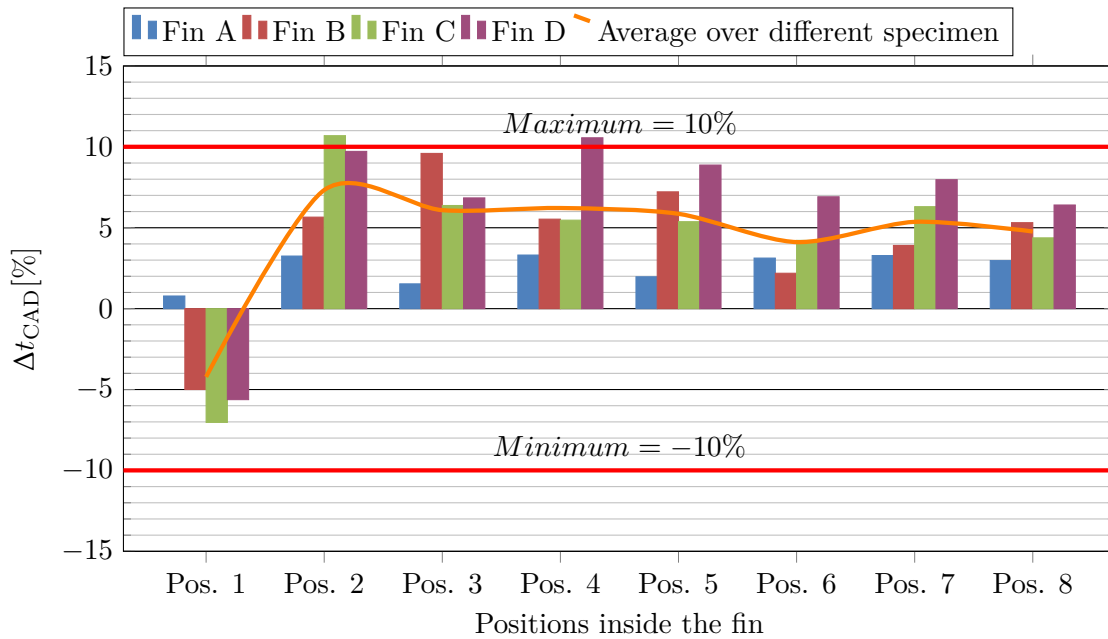


Figure 6.4.: Deviation between the average thickness and the desired thickness

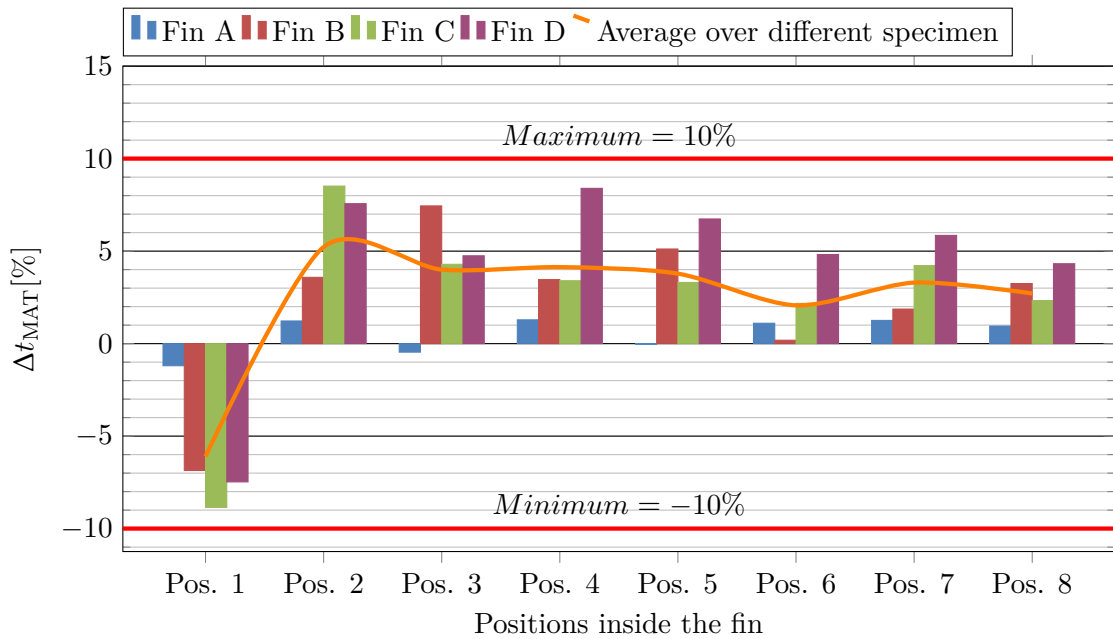


Figure 6.5.: Deviation between the average thickness and the thickness of the preform without compacting

In Pos. 1, some fibers get loose, because this position is exposed to rubbing in the process of vacuum and because the infrared emitter is striking more directly than in Pos. 8, overheating some fibers.

Looking at Figure 6.5, Fin D has in general wider deviations than the rest of the fins, which result in an increase of the average thickness profile (orange line). These deviations occur because the activation of the binder is not achieved over the entire surface, due to insufficient conditions of preforming. Fin C and fin D have a small wrinkle between Pos. 2 and Pos. 3, because the distance between both infrared emitters was big. This fact explains the deviations around these positions. Fin A hardly shows deviations because the preforming conditions were optimal regarding pressure, temperature, power...

Taking a deeper look at the columns of fin B and D, deviations go up and down along the positions and do not stay constant. A reason why, comes from a non-homogeneous heating taking place and as a result, there are positions where the binder was not properly activated (high deviations) and others, where the deviations are negligible. Fin A presents a consistent thickness along all the positions.

Another way to see the compaction of the part is by calculating the difference between the average thickness (\bar{t}) and the desired thickness (t_{CAD}) measured for every position. Dividing it by the number of layers and repeating this for the different positions, the

deviation per ply can be calculated and plotted, as seen in Equation 6.3 and Figure 6.6.

In Figure 6.7, this deviation is expressed in percentage.

$$\bar{t} - t_{CAD} \text{ per ply} = \frac{1}{\text{Number of positions}} \sum_{\text{Pos. } 1}^{\text{Pos. } 11} \frac{\bar{t} - t_{CAD}}{\text{Number of layers}} \quad (6.3)$$

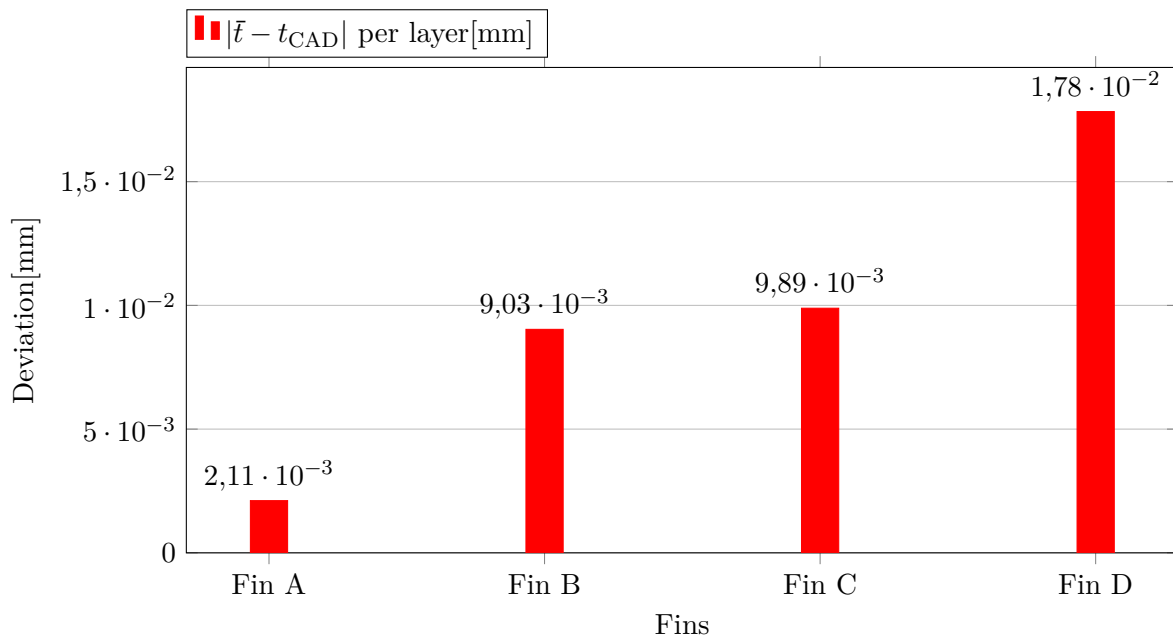


Figure 6.6.: Deviation in mm between measured thickness and desired thickness per layer

The results show that Fin A achieves the best results, obtaining a Minimum (Min.) thickness difference with respect to the desired thickness. Thus, fin D presents a bigger deviation with respect to the desired theoretical value. This is because the vacuum condition could not be made properly and because of the formation of a wrinkle around Pos. 2.

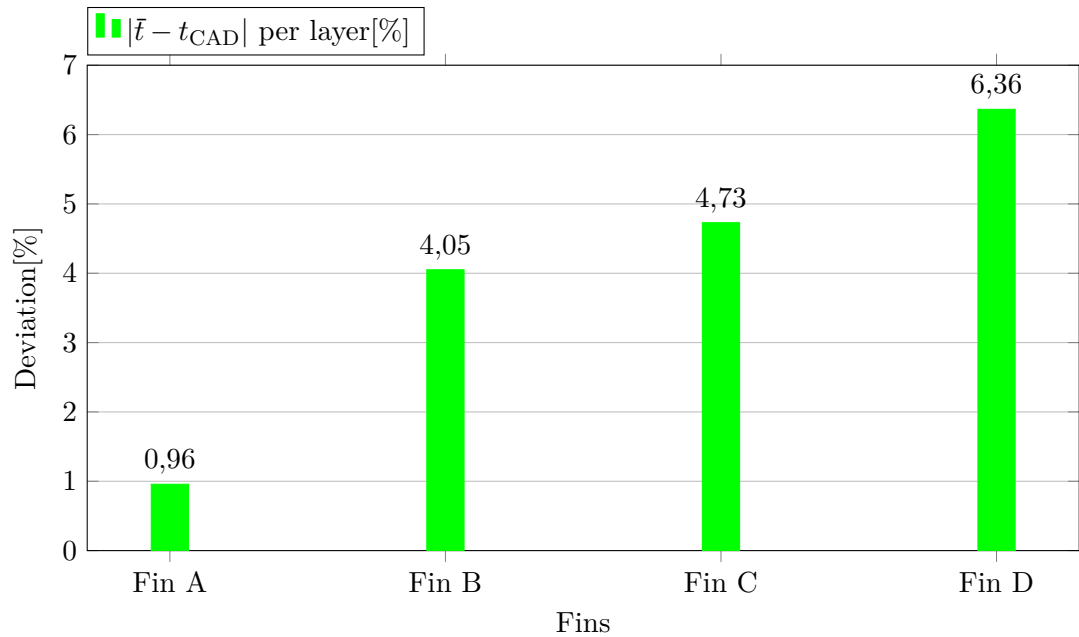


Figure 6.7.: Deviation in percentage between measured thickness and desired thickness per layer

The standard deviation (σ) can show us how the measurements taken can vary with respect to the average obtained. A large standard deviation (σ) may imply that there are irregularities in the surface, so it is not properly compacted. As it can be seen in Figure 6.8, the measurements of thickness in fin D do not converge very much in comparison with the other fins. The deviation in the values taken is due to the fact that the preform is not compacted uniformly in all its geometry and there are some differences between the values.

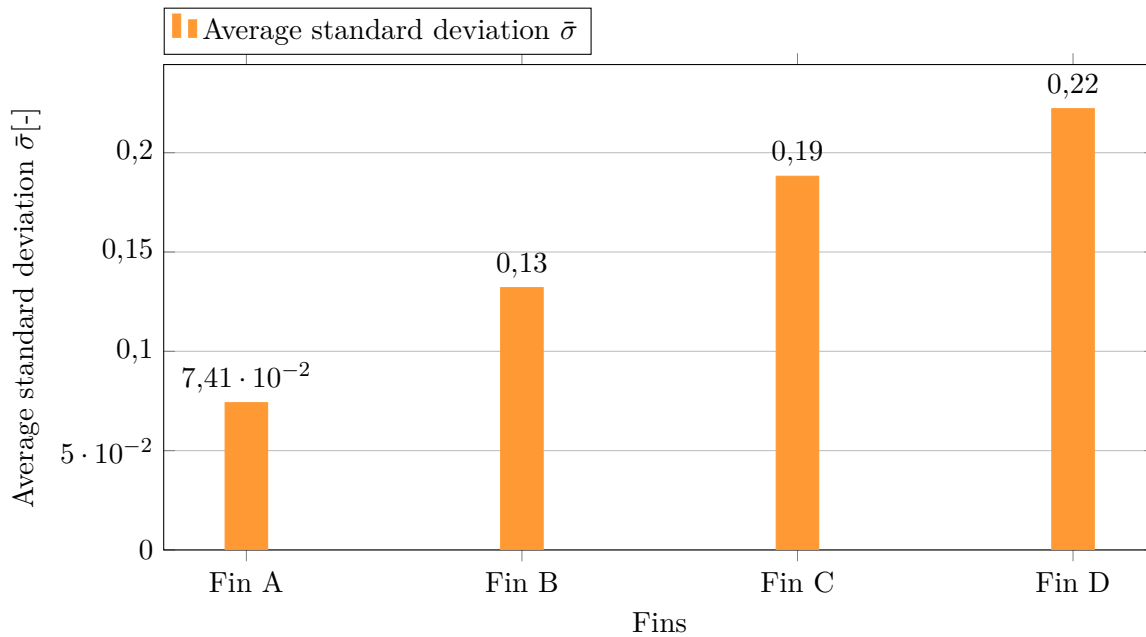


Figure 6.8.: Average standard deviation for every fin

6.2. Stiffness

Usually the displacement of a fin can be an indicator for the stiffness of the material. In the cantilever test, the compactness of the preform is measured by calculating the deflection of the fins as a beam, as it can be seen in Figure 6.9. No additional weight will be used: the part will deflect under its own weight.



Figure 6.9.: Fin C tested to deflection

Both the place of positioning the supports and the state of the fin determines the deflection. In this test, results can vary very much because of the flexibility of the materials and different results might be obtained. Nevertheless, the same conditions will be applied for all the fins tested and several measurements are taken in order to work with reasonable data.

As shown in Figure 6.10, the biggest deformations are found in fin D and the smallest deformations are found in Fin A. Comparing Figure 6.10 with Figure 6.6, it can be said that a good compaction and a binder activation (consolidation) result in good stiffness. Both figures show this connection and they are indications of the final quality, because when fin A makes short displacements, low deviations of thickness are reached too. On the contrary, it occurs with Fin D.

An indicator about the variation of the measurement is the standard deviation (σ). Thus, it can be seen that fin A gets a low data dispersion. This is because fin A is very compacted and the deflections measured do not differ from each other very much. On the other side, fin B and D, have large σ showing a low convergence in the results because these parts are very flexible, which makes it difficult to take uniform measurements.

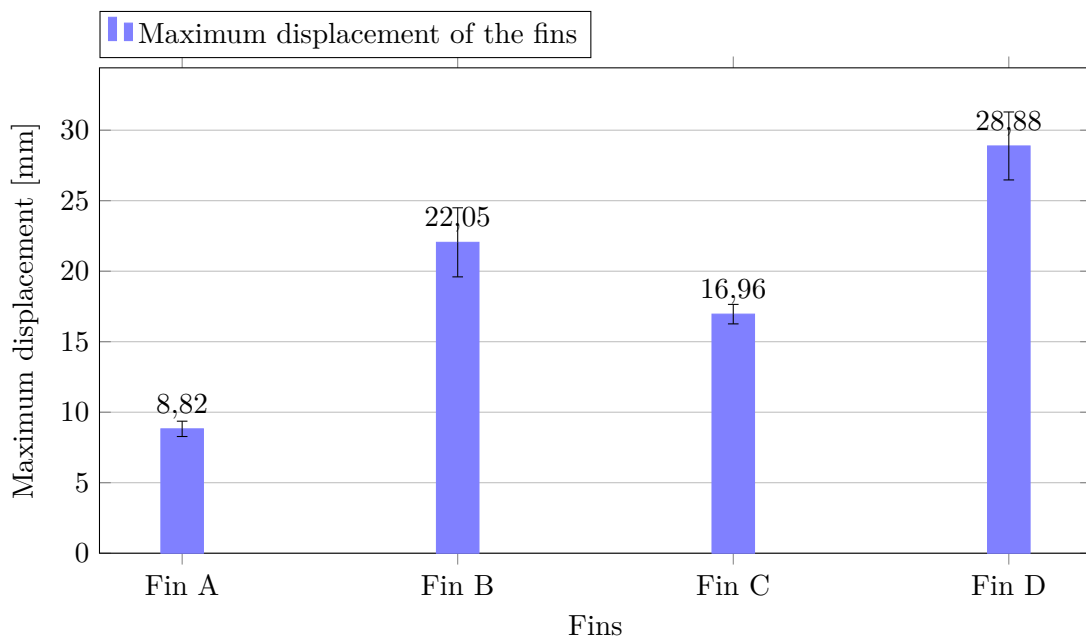


Figure 6.10.: Cantilever test fin

6.3. Length

Another requirement that is related to the quality of the preform is found in the length of the preform. As it will be explained later, one of the causes that leads to differences in the measurements of the length of the parts is the displacement of the layers. A good way to show if there are displacements among the plies is by measuring the actual length comparing it with the CAD value.

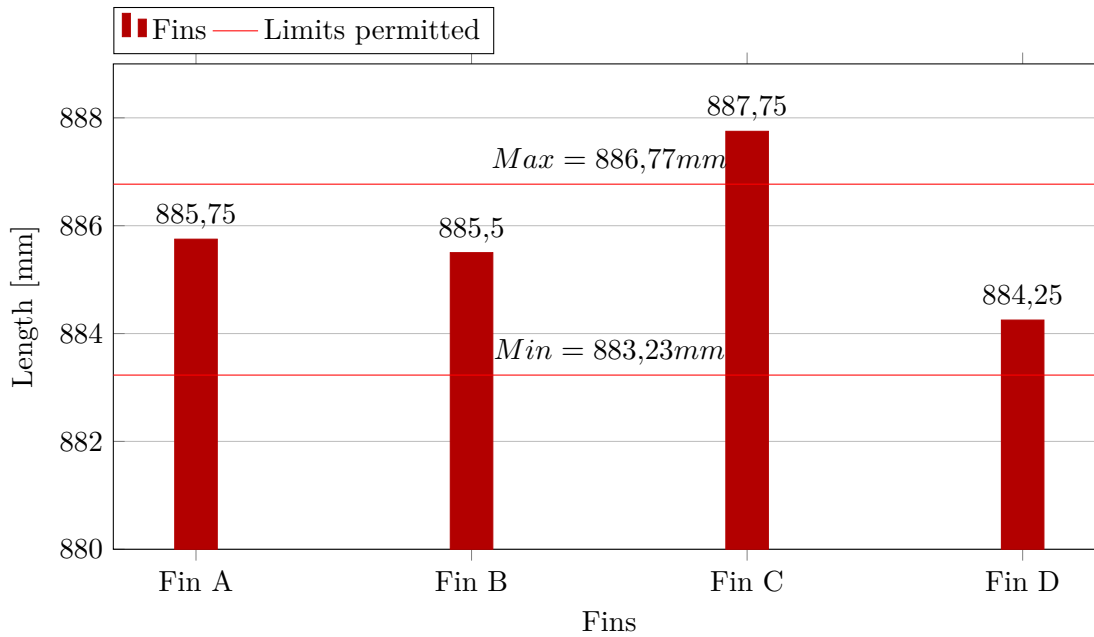


Figure 6.11.: Deviation along the actual length for the fins

In Figure 6.11, fin C diverges from the Maximum (Max.) value permitted because there was a displacement of the plies before heat was applied. According to [25, p. 7] a maximum deviation of ± 2 mm/m will be allowed. The reference CAD value for the fin is 885 mm. Fin A, B and D are included within this tolerance margin, and only Fin C differs from the established margin of 887,75 mm. This deviation is due to the displacement of layers, when creating the vacuum condition. A wrong initial alignment of the layers brings to deviations in the final result. Figure 6.12 shows that irregularity.



Figure 6.12.: Displacement between plies in the Fin C

Regarding the measurements of the C-Fin (Figure 6.13), both parts are within the length tolerances permitted and this is because the parts consist only of two plies of material and the adhesion can be better achieved than with many other plies. A good adhesion is important to prevent the displacement between plies.

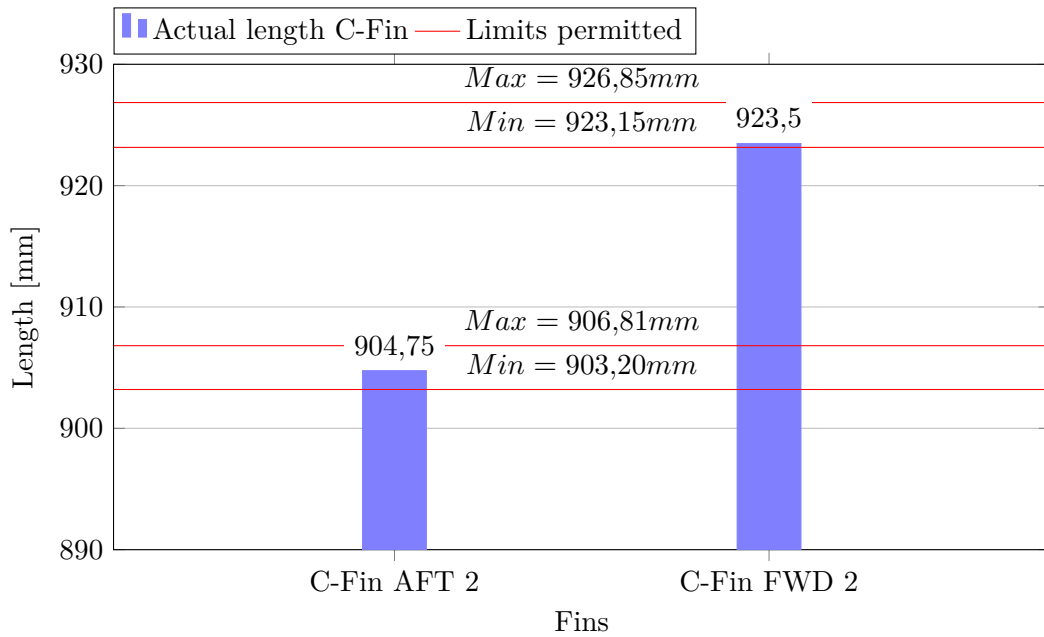


Figure 6.13.: Deviation along the actual length in the C-fins

Regarding L-Fin (Figure 6.14), L-Fin 1 was formed on the tooling created by the aircraft manufacturer, whereas L-Fin 2 was shaped on an aluminium plate.

Results differs from each other, as L-Fin 1 does not have any deviations because this part was created on the tooling provided by the aircraft manufacturer and this one has grooves which place the component exactly. L-Fin 2 was shaped on the aluminium plate and displacements between plies can occur as the preform is not placed inside grooves. As the deviation between the maximum limit allowed and the average obtained is 0,79 mm, the preform will not be discarded because the deviation is not excessive and the error is due to a wrong compaction of the plies, which makes them move slightly between the layers.

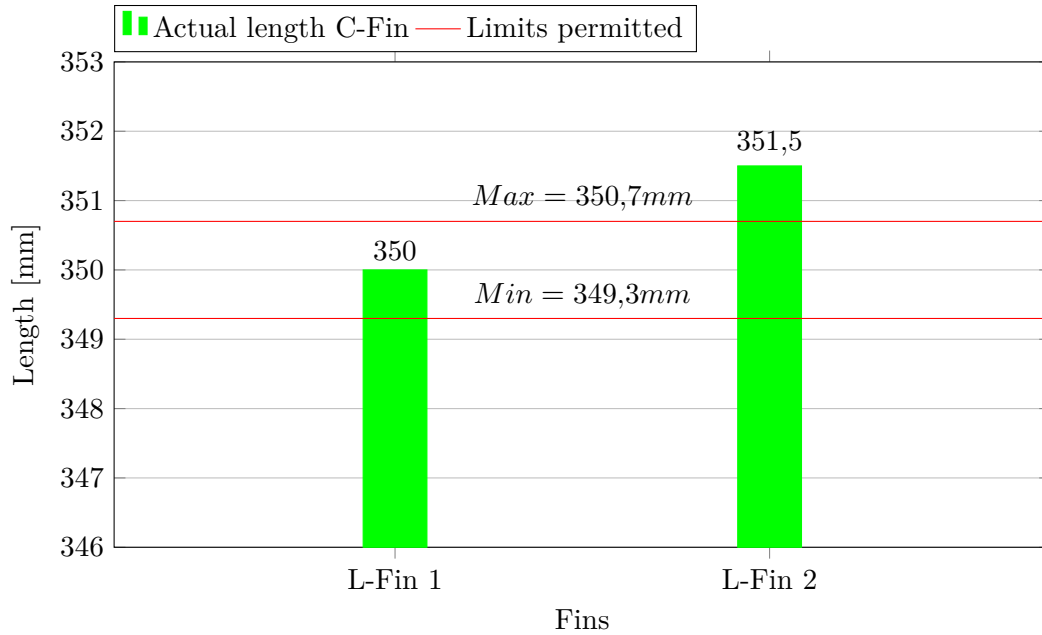


Figure 6.14.: Deviation along the actual length in the L-fins

Several conclusions can be drawn from the measurements of the actual length:

- Variation of the expected length is due to the displacement among plies when applying heat. Correct initial alignment is very important to avoid displacement between layers.
- The more plies there are, the easier a displacement between them will be, because binder might not be active in some plies. The measured length can differ from the expected one. Components with fewer plies show a better adhesion (e.g. C-Fins)
- In third place, the use of a tooling with grooves prevents the displacement of plies, although the border quality might be affected due to the contact between tooling and preform.

6.4. Optical analysis

To assess the quality of a preform a scale of 1 to 5 will be used. The fin will be scored for each of the requirements presented in [25]. A 5 corresponds to a "very widespread" aspect, a 1 to a "not found" aspect.

Fins

In fin A the guideline temperature provided by the manufacturer was slightly surpassed (around 130°C) and some outer fibers were loosened as a result. However, the fin was very well fixed and neither displacements among plies nor wrinkles took place because the fin was very well compacted.

Fin B is less rigid and compact than the fin A. In this fin the pressure and temperature conditions were good, but the application time was shorter than 20 minutes. This is the reason why this fin presents an insufficient adhesion of the plies in some positions. Upper plies are activated and some fibers are frayed because heat was being intensively applied on these positions.

In fin C, like in Fin B and Fin D, there were no overheated areas found because they were heated in the backwards where the powder binder is situated, so that carbon fiber areas are more protected. The final quality of the surface is very good, because temperature and pressure was very well controlled. However, there is a wrinkle between the plies because the distance between the infrared emitters was enlarged.

Although the last fin D presents a flexible behaviour and low compaction because the pressure of vacuum was not adequate, the visual quality of the surface is also good like in fin C. There are no overheated areas, displacements between layers or frayed fibers. Only a wrinkle is found in the middle of the fin because the distance between the infrared emitters was enlarged, like in fin C.

	Loosening single fibers	Overheating	Displacement among plies	Wrinkles, gaps	Poor adhesion of plies	Radius poorly formed	Overall quality
Fin A	3	3	1	1	1	/	1.80
Fin B	3-4	1	3	4	2-3	/	2.80
Fin C	1	1	1	4	2	/	1.80
Fin D	1	1	1	3	3	/	1.80

Table 6.1.: Visual requirements for the fins: 1) Aspect not found; 2) Aspect rarely found; 3) Aspect found in some specific points; 4) Aspect widespread; 5) Aspect very widespread

C-Fin AFT & C-Fin FWD

Results show that the C-Fins have an excellent quality. The fewer layers compacted, the easier it is to obtain a better final quality. The brilliant final quality of the front surface

is because the layers were ironed on the back side, so that the iron does not have any contact directly with the fibers.

	Loosening single fibers	Overheating	Displacement among plies	Wrinkles, gaps	Poor adhesion of plies	Radius poorly formed	Overall quality
C-Fin AFT	1	1	1	1	1	1	1
C-Fin FWD							

Table 6.2.: Visual requirements for C-Fin: 1) Aspect not found; 2) Aspect rarely found; 3) Aspect found in some specific points; 4) Aspect widespread; 5) Aspect very widespread

L-Fin 1 & L-Fin 2

Finally, L-Fin shows a different quality level, because the parts have been manufactured in different toolings. In L-Fin 1 no displacement between plies is reached because the preform is situated inside the grooves but the contact with the tooling influences in the preform make fibers get loose. On the other side, L-Fin 2 does not present any frayed fibers but a displacement in plies takes place because it is more difficult to fix the preform in the tooling.

	Loosening single fibers	Overheating	Displacement among plies	Wrinkles, gaps	Poor adhesion of plies	Radius poorly formed	Overall quality
L-Fin 1	4	2-3	1	1	1	1	1.75
L-Fin 2	2-3	1-2	3	1	1	1	1.67

Table 6.3.: Visual requirements for L-Fin: 1) Aspect not found; 2) Aspect rarely found; 3) Aspect found in some specific points; 4) Aspect widespread; 5) Aspect very widespread

6.5. Summary of the quality test

A study of the thickness of the preform in different positions shows how measurements vary in each fin. A position is compacted when there are not big variations between the measured thickness and the theoretical one. In general, in the preforms that were created, it is not a whole preform which differs from the desired value, but only some specific positions. When the binder has not been activated enough, the measured thickness can differ from the desired one. This can be due to a bad positioning of the heat source on

this position, or insufficient preforming conditions.

It was observed, that when there is a poor compaction, measurements in same positions can vary more than when there is a good compaction. Through the standard deviation (σ) the homogeneity of the measurements can be seen and with this, and provided that the material is in good condition, if the position was activated properly or not.

A way to assess the compaction of the component is by measuring the deflection of the preform under an applied load. If a part deflects in excess, that is because the preform is not compacted enough and the binder has not been activated properly.

Another conclusion that can be extracted is that preforming few plies gives better results than doing it with many plies. Binder is easier activated and the displacement between plies, due to the rubbing, can be reduced.

To achieve optimum preforming conditions, a combination of temperature, pressure, a suitable distance between radiators and the tests objects is required. Otherwise surface defects, such as wrinkles or burned fibers can appear.

7 Summary and outlook

The purpose of this work is the study of the quality and the reliability of the process for further new concepts. In particular the factors that influence the quality of the preforms will be analysed. Here, a tool will be built and the quality of the products will be studied. To heat the preforms, ironing, infrared method or a both methods will be combined to promote the activation of the binder. The materials used are NCF preforms with the different orientations.

In the tests of chapter 4 four flat fins are being tested on their manufacturing, one of which is made with optimal conditions of temperature, pressure and time of application. A lower heating time, a poor vacuum pressure or bad temperature conditions result in less compaction of the plies and the existence of non-activated zones.

The variation of distance of infrared emitters influences the result, like in the third fin, where an inadequate position of the infrared emitters leads to the presence of a wrinkle in the center of the fin.

For the manufacture of the L-shaped fin, the tool used has an impact on the final quality of the part. Ironing on an aluminum plate makes it possible, to achieve a higher temperature in the preform because it is not robust and the desired temperature can be reached easier. In addition, a better finish can be achieved. However, there is a risk of displacement between the plies as there are no grooves on the aluminium sheet. The existence of grooves fixes the preform in the tooling but the finish is worse since there is contact of the tool with the preform.

The manufacture of the C-fins brings incredible results since only two layers are ironed on the reverse and areas where the binder has not been activated (as well as displacements between plies) are easier avoided.

Moving to chapter 6, the compaction can be measured by the variation between the measured thickness and the desired thickness. The results show that in a poorly compacted fin, measurements of the same position can vary a lot. By means of the Cantilever test, which was carried out to test the stiffness of the preform, a relationship between stiffness and compaction is shown. The deviation between theoretical length and actual one was measured and proper securing is crucial to avoid possible initial movements between the

layers.

Finally, a visual study of quality was done to determine the causes of the appearance of defects in the preform were analyzed.

The tests carried out served to understand the influences that affect the manufacture of the preform and which defects appear when the initial conditions of preforming are modified.

As a solution for future trials, sensors could be installed on each layer to control the temperature and thus, to know if the temperature is adequate. And to avoid the displacement of layers in the fin, a flat mould with grooves could be used.

On the other hand, a study that may be very interesting is the thermal analysis of the preforms by finite elements in order to determine the estimated time to reach the desired temperature on the preform. This study may give the basis to achieve an optimal heating in order to avoid the overheating of fibers. Due to the limited time, a complete study could not be done in this work but a small test was applied with ANSYS to see the thermal distribution by conduction or infrared was included in Appendix A.4.

List of Figures

1.1. Factors of influence on the quality of the preform	3
2.1. NCF layout [12]	6
2.2. NCF used and orientations	6
2.3. Main production processes based on the component geometry [16, p. 13] .	7
2.4. Value chain of continuous fiber reinforced composites [17, p. 47]	8
2.5. RTM process for medium series[17, p. 13]	8
2.6. Deformation mechanisms of textile semi-finished products [20, p. 22] . . .	10
2.7. Preform technologies[21, p. 31]	10
3.1. Assembly of all components [13, p. 5]	13
3.2. Flap spars solids	14
3.3. Base geometries and final layout of the fin	15
3.4. Base geometries and final layout of the L-fin	16
3.5. Base geometries and final layout of the C-fin	16
3.6. Details of the tooling: a) Grooves on the lower cores; b) Aluminium plate folded; c) Cores of the tool; d) Assembly of the cores and the part together.	17
3.7. Support for infrared emitters	18
4.1. Activation of plies in the fin and thermal distribution	22
4.2. Final shape of fin B	22
4.3. Final shape of fin C	22
4.4. Final shape of fin D	23
4.5. Heat application on the L-fin 1 by means of an iron. An infrared emitter warms the surface of the tooling to promote the activation of the plies . .	23
4.6. Final shape of the L-Fin	24
4.7. Activation of plies in C-Fin and thermal distribution	24
4.8. Final shape of the C-Fin	25
5.1. Frayed fibers in the preform	27

5.2. An intensive heating can bring to the detachment of the fibers	28
5.3. Displacement of the plies in a preform	28
5.4. Gap and wrinkle found in the preform	29
5.5. Fin in profile	29
5.6. Angle measurement of a L-Fin	30
5.7. Plies fall out due to an insufficient adhesion	30
6.1. Fin layout and measurement positions	32
6.2. Average thickness of Fin A, Fin B, Fin C and Fin D for the different positions	32
6.3. Average thickness of the fin geometry for the different positions	33
6.4. Deviation between the average thickness and the desired thickness	34
6.5. Deviation between the average thickness and the thickness of the preform without compacting	35
6.6. Deviation in mm between measured thickness and desired thickness per layer	36
6.7. Deviation in percentage between measured thickness and desired thickness per layer	37
6.8. Average standard deviation for every fin	38
6.9. Fin C tested to deflection	38
6.10. Cantilever test fin	39
6.11. Deviation along the actual length for the fins	40
6.12. Displacement between plies in the Fin C	40
6.13. Deviation along the actual length in the C-fins	41
6.14. Deviation along the actual length in the L-fins	42
A.1. Disposition of the infrared emitters and measurements of the stand	66
A.2. Heat distribution for conduction and infrared radiation	67

List of Tables

2.1. Properties of matrix, fibers and as a composite [9]	5
3.1. Geometrical measurements for the aluminium sheet	17
3.2. Distribution of heat along the different preforms	19
6.1. Visual requirements for the fins: 1) Aspect not found; 2) Aspect rarely found; 3) Aspect found in some specific points; 4)Aspect widespread; 5)Aspect very widespread	43
6.2. Visual requirements for C-Fin: 1) Aspect not found; 2) Aspect rarely found; 3) Aspect found in some specific points;4)Aspect widespread;5)Aspect very widespread	44
6.3. Visual requirements for L-Fin: 1) Aspect not found; 2) Aspect rarely found; 3) Aspect found in some specific points; 4)Aspect widespread; 5)Aspect very widespread	44
A.1. Measurements of the stand and heating conditions for the fins	66
A.2. Temperature measurements on the surface of the fins during the heating .	66

Bibliography

- [1] LTD, Research ; MARKETS: *Growth Opportunities in Global Carbon Fiber Market 2016-2021*. <https://www.researchandmarkets.com/reports/3743269/growth-opportunities-in-global-carbon-fiber#>
- [2] *Carbon fiber vs aluminium - comprasion*. <http://www.dexcraft.com/articles/carbon-fiber-composites/aluminium-vs-carbon-fiber-comparison-of-materials/>
- [3] KÜHNEL, Michael ; KRAUS, Thomas: The global CFRP market 2016: Experience Composites. (Augsburg, September 21st 2016)
- [4] EDELMANN, Klaus: CFK-Thermoplast-Fertigung für den A350 XWB. In: *Lightweight Design* 5 (2012), Nr. 2, S. 42–47. <http://dx.doi.org/10.1365/s35725-012-0088-1>. – DOI 10.1365/s35725-012-0088-1. – ISSN 1865-4819
- [5] STAHL ; ARNE ; BORGWARDT ; HENRIK: *Quality Controlled Continuously Formed NCF-Preforms*. <http://elib.dlr.de/92682/>. Version: 05/06/2014
- [6] SCHÜRMAN, Helmut: *Konstruieren mit Faser-Kunststoff-Verbunden*. 2., bearbeitete und erw. Aufl. Berlin, Heidelberg : Springer-Verlag Berlin Heidelberg, 2007 (VDI-Buch). – ISBN 3540721908
- [7] QUINTERO, Liz: *FUNCIÓN DE LA MATRIZ EN MATERIALES COMPUESTOS*. undefined
- [8] DIAZ, A. ; GUIZAR-SICAIROS, M. ; POEPEL, A. ; MENZEL, A. ; BUNK, O.: Characterization of carbon fibers using X-ray phase nanotomography. In: *Carbon* 67 (2014), S. 98–103. <http://dx.doi.org/10.1016/j.carbon.2013.09.066>. – DOI 10.1016/j.carbon.2013.09.066. – ISSN 00086223
- [9] *undefined*. undefined
- [10] EMONTS M. ; JANSSEN H.: *Neue Technologien der Faserverbundtechnik: Potenzielle zukünftige Anwendungen für hochdynamische Vorschubsysteme*. Aachen, December 13th 2011

- [11] COMPOSITENCE: *Roving - Compositence*. <http://www.compositence.com/en/fiber-placement/innovation/roving/>
- [12] MAXXL2: *Multiaxial Fabrics*. https://upload.wikimedia.org/wikipedia/commons/thumb/f/fa/Multiaxial%7B_%7DFabrics.svg/2000px-Multiaxial%7B_%7DFabrics.svg.png
- [13] TAMAS HAVAR: *3 Point Bending Testing of FIN: LuFo IV: HIGHER-TE*, Diss., 16th Jan. 2013
- [14] COM, oandp: *Carbon Fiber: The More You Know, the More You Can Do - OPE-DGE.COM*. https://opedge.com/Articles/ViewArticle/2013-07_10
- [15] *Non Crimp Fabric | Danobat*. <http://www.drycomposites.com/tag/non-crimp-fabric/>
- [16] THOMAS KRAUS ; MICHAEL KÜHNEL ; ELMAR WITTEN: *Der Composites-Markt Europa: Marktentwicklungen, Herausforderungen und Chancen*.
- [17] LÄSSIG, R.: *Serienproduktion von hochfesten Faserverbundbauteilen: Perspektiven für den deutschen Maschinen- und Anlagenbau*. Studie Roland Berger, 2012
- [18] *RTM Process: J. Schmalz GmbH: Innovative Vacuum Technology from Schmalz*. <https://www.schmalz.com/en/applications/industries/composites/production-of-frp-components/rtm-process/>
- [19] *Resin transfer moulding for aerospace structures*. [Place of publication not identified] : Springer, 2013. – ISBN 9401144370
- [20] NOSRAT NEZAMI, Farbod: *Automatisiertes Preforming von Kohlefaserhalbzeugen mit aktiven Materialführungssystemen zur Herstellung komplexer Faserverbundstrukturen*. 1. Aufl. Berlin : epubli GmbH, 2015. – ISBN 9783737561853
- [21] MACK, Jens: *IVW-Schriftenreihe*. Bd. Bd. 115: *Entwicklung eines adaptiven Online-Bebinderungsprozesses für die Preformherstellung*. Als Ms. gedr. Kaiserslautern : IVW, 2015. – ISBN 978-3-944440-11-8
- [22] ONLINE, FOCUS: *Leicht ist und wird es auch nicht*. https://www.focus.de/auto/neuheiten/tid-18873/bmw-megacity-vehicle-leicht-ist-und-wird-es-auch-nicht_aid_525182.html. Version: 12/09/2010

- [23] ROHATGI, Vivek ; LEE, L. J.: *Moldability of Tackified Fiber Preforms in Liquid Composite Molding*. <http://journals.sagepub.com/doi/abs/10.1177/002199839703100705>. Version: 27/07/2016
- [24] TEMPEL ALFRED: *FLB-Kolloquium: Vorstellung Projekt Next.Move*. Braunschweig, 23.05.2016
- [25] TEMPEL ALFRED: *Lastenheft Next.Move AP2300: Version 1.1: DLR*. 04.05.16
- [26] *EASYGLISS 30 AUTO-OFF*. <https://www.tefal.se/K1%C3%A4dv%C3%A5rd/%C3%85ngstrykj%C3%A4rn/Efficient/EASYGLISS-30-AUTO-OFF/p/2820403050>
- [27] *Carbon Infrared Heaters*. https://www.heraeus.com/us/hng/products_and_solutions/heraeus_noblelight_america/infrared_heaters/standard_infrared_heaters/carbon_infrared_heaters.aspx
- [28] KITTLASS, Eckhard: DIVAC: Diaphragm Vacuum Pumps: 171.02.02. In: *Full Line Catalog SectionC04* (2010)
- [29] LEYBOLD GMBH: *Digitales PIEZOVAC-Vakuummeter PV 101 | Leybold*. <https://www.leyboldproducts.de/produkte/vakuu-messen/handmessgeraete/2667/digitales-piezovac-vakuummeter-pv-101>

A Appendix

A.1. Technical data sheets

A.1.1. Dry Reinforcements Woven Fabric

Bidirectional fabric basic

||| Toho Tenax |

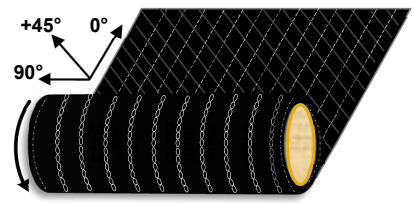
TEIJIN

Technical Data Sheet
Tenax® Dry Reinforcements Non-Crimp Fabric

Brand name	Tenax®
Production site	E (Europe)
Product family	DRNF
Product designation	PB11_07-V8_05-IMS65-BD1-TP22-0388-1270
Article Number	7410c005_051
Type of Textile	Bidiagonal Non-Crimp Fabric – Basic
Textile areal weight (incl. sizing, binder, toughener, etc.)	407g/m ² ± 20g/m ²
Carbon fibre areal weight (incl. sizing)	388g/m ² ± 19g/m ²

NCF detail construction

Layer	Material	Areal weight [g/m ²]
5	Powder Binder Hexion EP05311	7
4	Toughener TA1902	5
3	-45° Carbon Fibre: Tenax®-E IMS65 E23 24K 830tex	194
2	Toughener TA1902	5
1	+45° Carbon Fibre: Tenax®-E IMS65 E23 24K 830tex	194

Stitching yarn	CoPa	2.0
Weave	Tricot-Pillar	 <p>Fibre-Orientation in acc. to EN13473-1</p>
Stitching length	2.2 mm	
roll dimension	Paper core: 152mm Fabric width: 1270mm Length: typ. 50m	

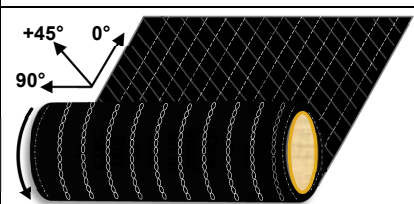
Preforming recommendation: Apply vacuum on preform package and hold for 20min at 120°C.

Toughening system: The Non-woven based toughening system TA1902 is developed for all resin infusions processes with curing temperature of ca. 180°C.

Brand name	Tenax®
Production site	E (Europe)
Product family	DRNF
Product designation	PB11_07-V8_05-IMS65-BD2-TP22-0388-1270
Article Number	7411c005_051
Type of Textile	Bidiagonal Non-Crimp Fabric – Symmetrical
Textile areal weight (incl. sizing, binder, toughener, etc.)	407g/m ² ± 20g/m ²
Carbon fibre areal weight (incl. sizing)	388g/m ² ± 19g/m ²

NCF detail construction

Layer	Material	Areal weight [g/m ²]
5	Powder Binder Hexion EP05311	7
4	Toughener TA1902	5
3	+45° Tenax®-E IMS65 E23 24K 830tex	194
2	Toughener TA1902	5
1	- 45° Tenax®-E IMS65 E23 24K 830tex	194

Stitching yarn	CoPa	2.0
Weave	Tricot-Pillar	 <p>Fiber-Orientation in acc. to EN13473-1</p>
Stitching length	2.2 mm	
roll dimension	Paper core: 152 mm	
	Fabric width: 1270 mm Length: custom made (typ. 50m)	

Preforming recommendation: Apply vacuum on preform package and hold for 20min at 120°C.

Toughening system: The Non-woven based toughening system TA1902 is developed for all resin infusions processes with curing temperature of ca. 180°C.

The export or transfer of carbon fibre products can be subject to authorisation, depending on end-use and final destination.

A.1.2. Infrared heater

Technische Daten

Zwillingsrohrstrahler	kurzwellig	schnell mittelwellig	mittelwellig	Carbon
Max. Leistung W/cm	< 200	80	18/20/25*	60
Max. beheizte Länge mm	6400/2400*	6400/2400*	1500/2000/6500*	3000
Querschnitt mm	34 x 14	34 x 14	18 x 8	34 x 14
	23 x 11	23 x 11	22 x 10	
			33 x 15	
Filament-Temperatur °C	1800–2400	1400–1800	800–950	1200
Wellenlänge µm	1.0–1.4	> 1.4	2.4–2.7	2
Max. Flächenleistung kW/m ²	200	150	60	110
Reaktionszeit s	1	1–2	60–90	1–2

* Abhängig vom Querschnitt

Goldene 8 Standardstrahler

	Leistung [Watt]	Spannung [Volt]	beheizte Länge [mm]	Gesamtlänge [mm]	Strahlertyp	Artikelnummer
Mittelwelle	500	230	300	400	B	09752439
	1000	230	500	600	B	09755167
	2000	230	800	900	B	09755054
	2500	230	1000	1100	B	09755255
	3250	230	1300	1420	B	09753187
	3750	230	1500	1600	B	09754585
	4100	400	1700	1800	B	09754863
	4500	400	1800	1920	B	09754783
	5750	400	2300	2400	B	09756083
	6250	400	2500	2600	B	09753874
Kurzwelle	2500	230	1200	1300	C	09753923
	3000	400	1000	1100	A	09751720
	600	115	80	145	B	09751713
	1500	230	200	300	B	09751751
	1200	230	340	405	B	09751741
	3000	400	500	600	B	09751740

Source: [27, p. 9]

A.1.3. Vacuum pump

Source:[28, p. 7]

Technical Data

		0.6	DIVAC 1.2	2.2
Max. pumping speed (atm.)	m ³ x h ⁻¹ (cfm)	0.6 (0.4)	1.2 (0.7)	2.0 (1.2)
Ultimate pressure	mbar (Torr)	≤ 100 (≤ 75)	≤ 100 (≤ 75)	≤ 100 (≤ 75)
Max. exhaust back pressure (absolute)	mbar (Torr)	2000 (1500)	2000 (1500)	2000 (1500)
Pump heads		1	1	1
Connection				
Inlet (suction side)	DN	Hose nozzle ID 10	Hose nozzle ID 10	Hose nozzle ID 10
Exhaust (delivery side)	DN	Hose nozzle ID 10	Hose nozzle ID 10	Hose nozzle ID 10
Thread (suction and delivery side)	G	G 1/8"	G 1/4"	G 1/4"
Noise level acc. to DIN 45 635 Part 13, approx.	dB(A)	47	50	52
Permissible gas admission temperature, max.	°C (°F)	+5 to +40 (+41 to +104)	+5 to +40 (+41 to +104)	+5 to +40 (+41 to +104)
Permissible ambient temperature, max.	°C (°F)	+5 to +40 (+41 to +104)	+5 to +40 (+41 to +104)	+5 to +40 (+41 to +104)
Voltage / nominal frequency (1 ph. motor)				
Schuko plug	V / Hz	230 ± 10% / 50	230 ± 10% / 50	230 ± 10% / 50
NEMA plug	V / Hz	115 ± 10% / 60	115 ± 10% / 60	115 ± 10% / 60
NEMA plug	V / Hz	100 ± 10% / 50/60	100 ± 10% / 50/60	100 ± 10% / 50/60
Protective class	IP	44	44	44
Motor power ¹⁾	W	100	130	180
Current consumption ¹⁾	A	0.6	0.9	1.35
Motor speed				
50 Hz	min ⁻¹	1500	1500	1500
60 Hz	min ⁻¹	1800	1800	1800
Dimensions (W ¹⁾ x H ¹⁾ x D), approx.	mm (in.)	256 x 146 x 187 (10.08 x 5.75 x 7.36)	268 x 159 x 207 (10.55 x 6.3 x 8.15)	297 x 171 x 226 (11.69 x 6.73 x 8.9)
Weight, approx.	kg (lbs)	5.9 (13.02)	7.1 (15.57)	10.3 (22.74)
Material				
Pump head		PTFE (Teflon)	PTFE (Teflon)	PTFE (Teflon)
Structured diaphragm		PTFE coated	PTFE coated	PTFE coated
Valves		FFPM (Kalrez)	FFPM (Kalrez)	FFPM (Kalrez)
Nozzles		PVDF (Solef)	PVDF (Solef)	PVDF (Solef)

Ordering Information

	0.6	DIVAC 1.2	2.2
Diaphragm vacuum pump 230 V, 50 Hz, with 2.3 m (8 ft) power cord and Schuko plug	Part No. 127 60	Part No. 127 61	Part No. 127 62
Spare parts kit consisting of 1 diaphragm, 2 gasket rings, 2 valve disks	Part No. 127 63	Part No. 127 64	Part No. 127 65
Hose nozzles 1 exhaust port and 2 inlet ports	Part No. 200 650 25 (2x)	Part No. 200 650 26 (2x)	Part No. 200 650 26 (2x)

¹⁾ for 230 V / 50 Hz version

A.1.4. Digital barometer

VacuGraph Zubehör-Set

Technische Daten



THERMOVAC TM 101 mit VacuGraph-Zubehörset

VacuGraph Zubehör-Set (Optional)

Das Zubehörset ist in einem praktischen Koffer untergebracht und umfasst Software, USB Schnittstellenkabel und Adapter. Alle Teile sind darin geschützt und an einem Platz.

Die intelligente Software erlaubt neben der Messdatenaufzeichnung ein Auslesen der Datenspeicher des PIEZOVAC PV 101 und THERMOVAC TM 101. Die Messdaten können als Diagramm ausgedruckt oder für weitere Auswertungen als Textdatei exportiert werden.

Besondere Vorteile des Zubehör-Sets sind:

- Einfache Aufbewahrung und Transport
- Schnelle und einfache Anpassung von Kennzahlen
- Datenaufzeichnung und Visualisierung für weitere Analysen
- Einfache Einstellung von Parametern wie Aufzeichnungsrate, Messeinheit oder Gaskorrekturfaktor
- Alle Teile sind geschützt und an einem Platz

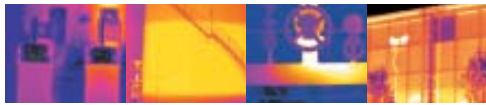
Technische Daten	PIEZOVAC PV 101	THERMOVAC TM 101
Messprinzip (gasartabhängig)	Piezoresistiv	Piezoresistiv und Wärmeleitfähigkeit Pirani
Darstellbare Messeinheiten	mbar, Torr, Pa	mbar, Torr, Pa
Messbereich	1200 - 0,1 mbar	1200 bis $5 \cdot 10^{-4}$ mbar
Messgenauigkeit	0,3 % f.s. vom Skalen-Endwert	0,3 % f.s. vom Skalen-Endwert
bei 1200 - 10 mbar	–	10 % vom Messwert
bei $10 - 2 \times 10^{-3}$ mbar	–	< Faktor 2
< 2×10^{-3} mbar		
Messzyklus	100 ms	1,6 s
Spannungsversorgung	Akku 9V Batterie oder 15 V DC Stecker-Netzteil	Akku 9V Batterie oder 15 V DC Stecker-Netzteil
Leistungsaufnahme < 200 mbar / > 200 mbar	60 mW / 0,5 mW	60 mW / 0,5 mW
Betriebsdauer 6 LR61 Alkali (Vakuumbetrieb)	< 2500 h	bis zu 75 h
Anzeige	LCD 12 mm	LCD 12 mm
Anschluss (Edelstahl)	G1/4" Innengewinde (DN16 ISO KF mit Adapter)	DN 16 ISO-KF
PC-Schnittstelle	Mini-USB, Typ B, 5-Pin, Innengewinde Virtual COM-Port Protokoll	Mini-USB, Typ B, 5-Pin, Innengewinde Virtual COM-Port Protokoll
Abmessungen (ohne Flansch)	60 x 120 x 25 mm	60 x 120 x 25 mm
Schutzart	IP 40	IP 40
Gewicht (inkl. Batterie)	200 g	230 g
Bestellinformation	PIEZOVAC PV 101	THERMOVAC TM 101
Handmessgerät, DN 16 ISO-KF inklusive AIMn-Batterie, 9V Block 6LR61	Kat. Nr. 230 080 V01	Kat. Nr. 230 081 V01
VacuGraph Windows Software-Zubehörset in Schutzkoffer mit Schaumstoff-Einlage. Inklusive USB-Schnittstellenkabel (2 m), Stecker-Netzteil 15 V für Netzspannung 100-260 V, 50/60 Hz und AIMn-Batterie, 9V Block 6LR61	Kat. Nr. 230 082 V01	Kat. Nr. 230 082 V01



Leybold GmbH
Bonner Str. 498 · D-50968 Köln
T +49 (0) 221-347-0

Source: [29, p. 4]

A.1.5. Thermal camera



TECHNICAL SPECIFICATIONS

IMAGING PERFORMANCE

Field of view/min focus distance	25° x 19°/0.3 m
Thermal sensitivity	0.12°C at 25°C
Image frequency	50/60 Hz non-interlaced
Focus	Manual
Detector type	Focal Plane Array (FPA), uncooled microbolometer
	160 x 120 pixels, vanadium oxide
	7.5 to 13 µm
	300:1

minimum diameter measurement
spot at 10 cm (with 45° lens)

IMAGE PRESENTATION

Video output	PAL or NTSC, standard RCA composite video
External display	2.5" colour LCD, 16K colors

MEASUREMENT

Temperature range	-20°C to +250°C, (-4°F to +482°F) up to +900°C optional
Accuracy	±2°C, ±2%
Repeatability	±1°C, ±1%
Measurement mode	3 movable spots, area max, area min, area average, color alarm above or below Palettes (iron, rainbow, B&W, B&W invers), auto-adjust (continuous/manual)
Menu controls	Date/time, temperature units °C/°F, language, scale, info field, LCD intensity (high/normal/low)
Set-up controls	Emissivity variable from 0.1 to 1.0, reflected ambient
Measurement corrections	

IMAGE STORAGE

Type	Built-in FLASH memory (up to 100 images)
File formats	Standard JPEG

LENSES (OPTIONAL)

2 x Telescope (12° x 9"/1.2 m)
0.5 Wide angle (45° x 34"/0.1 m)



adapt your camera
to EVERY situation

LASER LOCATIR™

Classification	Class 2
Type	Semiconductor AlGaInP Diode Laser: 1mW/635 nm red

BATTERY SYSTEM

Type	Li-Ion, rechargeable, field replaceable
Operating time	2 hours continuous operation. Display shows battery status
Charging system	In camera, AC adapter or 12 V from car (with optional Std. cable) 2 bay intelligent charger, 12 V AC adapter 90-260 V AC, 50/60 Hz, 12 V DC out 11-16 V DC
AC operation	Automatic shutdown and sleep mode (user selectable)
Voltage	
Power saving	

ENVIRONMENTAL SPECIFICATION

Operating temperature range	-15°C to +45°C (+5°F to +113°F)
Storage temperature range	-40°C to +70°C (-40°F to +158°F)
Humidity	Operating and storage 20% to 80%, non-condensing
Encapsulation	IP54 IEC 359
Shock	Operational: 25G, IEC 68-2-29
Vibration	Operational: 2G, IEC 68-2-6

PHYSICAL CHARACTERISTICS

Weight	700 g (1.5 lbs.), incl. battery with 25° lens
Size	265 mm x 80 mm x 105 mm (10.4" x 3.1" x 4.1")
Tripod Mounting	1/4" - 20
Cover case	Plastic and rubber

INTERFACES

USB	Image transfer to PC
RS-232 cable (optional)	Image transfer to PC
Video Output	Standard RCA composite video

ThermaCAM E4 includes:

IR camera, Carrying case, Power supply, Handstrap, Lens cap, ThermaCAM Connect™ Software,
USB cable, User manual, Power cord, Battery, Battery charger

SPECIFICATIONS ARE SUBJECT TO CHANGE WITHOUT NOTICE

© Copyright 2003, FLIR Systems, Inc. All other brand and product names are trademarks of their respective owners



FLIR Systems AB

World Wide Thermography Center
Rinkebyvägen 19 - PO Box 3
SE-182 11 Danderyd
Sweden
Tel.: +46 (0)8 753 25 00
Fax: +46 (0)8 753 23 64
e-mail: sales@flir.se
www.flir.com

FLIR Systems Ltd.

United Kingdom
Tel.: +44 (0)1732 220 011
e-mail: sales@flir.uk.com

FLIR Systems Co. Ltd.

Hong Kong
Tel.: +852 27 92 89 55
e-mail: flir@flir.com.hk

FLIR Systems GmbH

Germany
Tel.: +49 (0)69 95 00 900
e-mail: info@flir.de

FLIR Systems Sarl

France
Tel.: +33 (0)1 41 33 97 97
e-mail: info@flir.fr

FLIR Systems S.r.l.

Italy
Tel.: +39 02 39 09 121
e-mail: info@flir.it

FLIR Systems AB

Belgium
Tel.: +32 (0)3 287 87 11
e-mail: info@flir.be

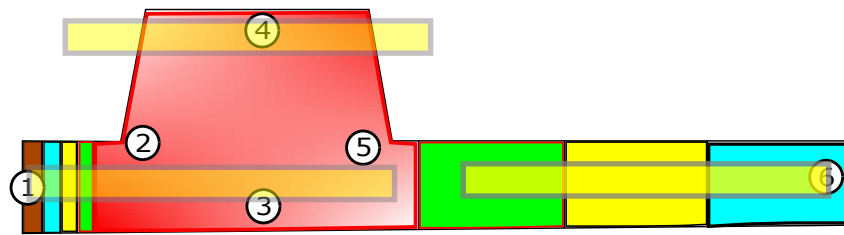
www.flir.com



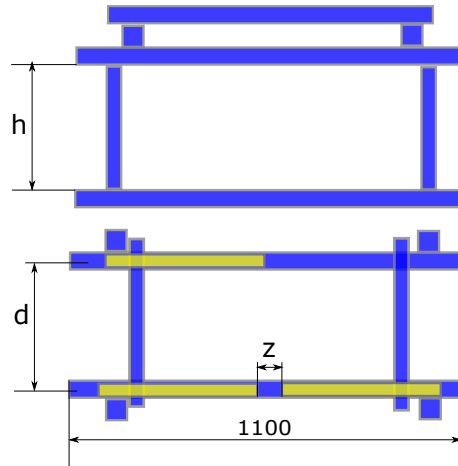
A.2. Stacking sequence woven fabrics

10			5			5			2					
Fin			LFimFWD			LFimAFT			CFimFWD			CFimAFT		
Mat.	Orient.	Geom.	Mat.	Orient.	Geom.	Mat.	Orient.	Geom.	Mat.	Orient.	Geom.	Mat.	Orient.	Geom.
BiaxTT	+45	Fin_1	BiaxTT	+45	LFimFWD	BiaxTT	+45	LFimAFT	TriaxTT	-45	CFimFWD_1	TriaxTT	-45	CFimAFT_1
BiaxTT	-45		BiaxTT	-45		BiaxTT	-45		TriaxTT	90		TriaxTT	90	
BiaxTT	0	Fin_2	BiaxTT	90	LFimFWD	BiaxTT	0	LFimAFT	BiaxTT	+45	CFimFWD_2	BiaxTT	0	CFimAFT_2
BiaxTT	+45		BiaxTT	+45		BiaxTT	+45		BiaxTT	90		BiaxTT	90	
BiaxTT	-45	Fin_3	BiaxTT	-45	LFimFWD	BiaxTT	-45	LFimAFT	BiaxTT	0	LFimFWD	BiaxTT	0	CFimAFT
BiaxTT	+45		BiaxTT	+45		BiaxTT	+45		BiaxTT	90		BiaxTT	90	
BiaxTT	0	Fin_4	BiaxTT	90	LFimFWD	BiaxTT	90	LFimAFT	BiaxTT	-45	LFimFWD	BiaxTT	-45	CFimAFT
BiaxTT	+45		BiaxTT	+45		BiaxTT	+45		BiaxTT	90		BiaxTT	90	
BiaxTT	-45	Fin_5	BiaxTT	-45	LFimFWD	BiaxTT	-45	LFimAFT	BiaxTT	0	LFimFWD	BiaxTT	0	CFimAFT
BiaxTT	+45		BiaxTT	+45		BiaxTT	+45		BiaxTT	90		BiaxTT	90	

A.3. Temperature measurements and data about the heating conditions



(a) Position of infrared emitters along the fin



(b) Stand layout

Figure A.1.: Disposition of the infrared emitters and measurements of the stand

	Fin A	Fin B	Fin C	Fin D
h (mm)	220	100	200	200
d (mm)	160	160	160	160
z (mm)	5	5	9	9
Pressure (mbar)	466	225	480	529
Heating time (min)	65	20	30	30

Table A.1.: Measurements of the stand and heating conditions for the fins

	Fin A		Fin B	Fin C	Fin D
Power %	40	60	20-30	30	30
Position	Temperatures on the surface (°C)				
1	92.6	99.1	105.9	107.7	101.9
2	95	116.2	90.8	109.8	116.3
3	117.8	126.9	127.9	137.9	124.7
4	123.8	135.5	118.8	137.5	141.5
5	122.4	134.9	97.9	91	90.2
6	78.6	85.9	68.6	87	90.7

Table A.2.: Temperature measurements on the surface of the fins during the heating

A.4. ANSYS Simulation: Heat distribution along the fin

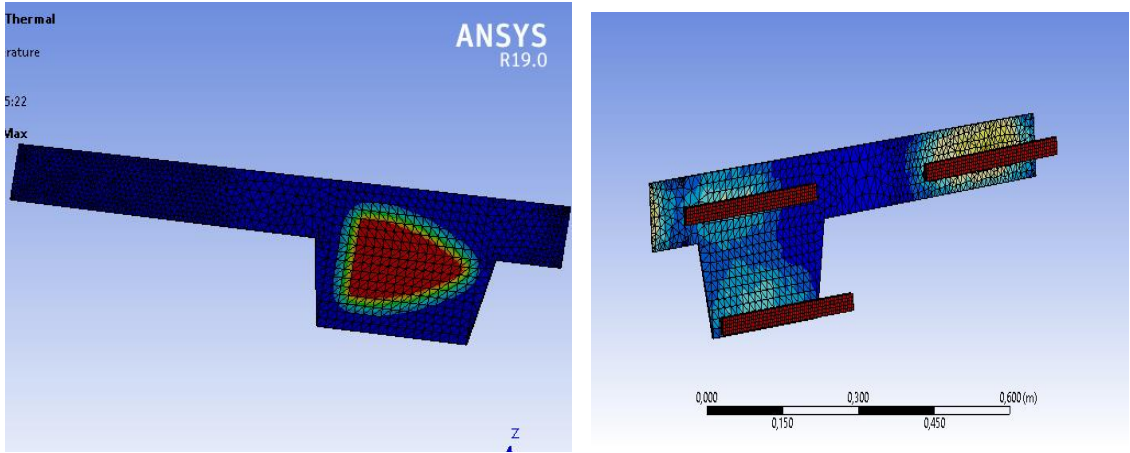


Figure A.2.: Heat distribution for conduction and infrared radiation